Journal of Medicinal Chemistry

Article

Phthalocyanines and tetrapyrazinoporphyrazines with two cationic donuts: high photodynamic activity as a result of rigid spatial arrangement of peripheral substituents

Basma Ghazal, Miloslav Machacek, Mona Abbas Shalaby, Veronika Novakova, Petr Zimcik, and Saad Makhseed

J. Med. Chem., **Just Accepted Manuscript** • Publication Date (Web): 30 May 2017

Just Accepted

ACS Publications

Journal of Medicinal Chemistry is published by the American Chemical Society. 1155 Sixteenth Street N.W., Washington, DC 20036

Phthalocyanines and tetrapyrazinoporphyrazines with two cationic donuts: high photodynamic activity as a result of rigid spatial arrangement of peripheral substituents

Basma Ghazal,† Miloslav Machacek,‡ Mona Abbas Shalaby,† Veronika Novakova,§ Petr Zimcik,‖ and Saad Makhseed*,†*

†Department of Chemistry, Kuwait University, P.O. Box 5969, Safat, 13060, Kuwait

‡Department of Biochemical Sciences, Faculty of Pharmacy in Hradec Kralove, Charles University in Prague, Heyrovskeho 1203, Hradec Kralove, 500 05, Czech Republic

§Department of Biophysics and Physical Chemistry, Faculty of Pharmacy in Hradec Kralove, Charles University in Prague, Heyrovskeho 1203, Hradec Kralove, 500 05, Czech Republic

‖Department of Pharmaceutical Chemistry and Pharmaceutical Analysis, Faculty of Pharmacy in Hradec Kralove, Charles University in Prague, Heyrovskeho 1203, Hradec Kralove, 500 05, Czech Republic

ABSTRACT

High photodynamic activity was observed for hexadeca-cationic zinc, magnesium and metal-free phthalocyanines (Pcs) and tetrapyrazinoporphyrazines with EC_{50} values as low as 5 nM (MCF-7 cells) for the best compound; this activity was several times better than that of clinically established photosensitizers verteporfin, temoporfin, S_3AlOHPc or protoporphyrin IX. This lead compound was characterized by low dark toxicity (TC_{50} = 369 μM), high efficiency against other cell lines (HCT 116 and HeLa) and possible activation by light above 680 nm. The excellent photodynamic activity resulted from the rigid spatial arrangement of the quaternized triazole moieties above and below the Pc core, as confirmed by X-ray crystallography. The triazole moieties thus formed two "cationic donuts" that protected the hydrophobic core against aggregation in water. The lysosomes were found to be the site of subcellular localization and were consequently the primary targets of photodynamic injury, resulting in predominantly necrotic cell death.

INTRODUCTION

Photodynamic therapy (PDT) is a relatively modern cancer treatment used as an alternative to chemotherapy, radiotherapy and surgical intervention. PDT combines three potentially nontoxic components—light, oxygen, and a photosensitizer (PS)—that are able to destroy target cells by the production of toxic species, the most important being singlet oxygen.[1] PSs from various structural groups have been approved for use in clinical practice or are under investigation in clinical trials.[2] The key photophysical characteristics of an efficient PS are good production of singlet oxygen and strong absorption of light in the optical window of tissues (or phototherapeutic window, *i.e.,* 650-850 nm), where the penetration of light is the deepest.[3] From this point of view, phthalocyanines (Pcs), which typically possess very good singlet oxygen production and extinction coefficients over 2×10^5 M^{-1} cm^{-1} are interesting molecular structures.[4,5] Indeed, sulfonated hydroxyaluminum Pc with an average degree of sulfonation n = 3 (S_3AlOHPc) has been approved in Russia since 2001.[5,6] On the other hand, the Pc core is planar and strongly hydrophobic; as a result, it tends to form strong aggregates in water and water-based media, which can substantially reduce or completely eliminate the photophysical pathways important for PDT. Several strategies on how to resolve this obstacle have been developed by various research groups. The strategies include the use of surfactants/co-solvents[7,8] or delivery systems[9-11] to dissolve the lipophilic compounds or substitution by highly hydrophilic substituents axially on the central metal[12,13] or on the Pc core.[14-17]

Recently, we identified Pcs with rigid cationic substituents bearing quaternized imidazolyl moieties, which led to highly water-soluble Pcs that did not display any aggregation in water.[18] Applying the same substituents to tetrapyridoporphyrazines resulted in a compound that belongs among the most potent

PSs reported to date.[19] Considering the promising anticancer photodynamic activity of these PSs bearing imidazolyl moieties, we applied the same protocol to prepare triazole-containing Pc complexes and anticipated obtaining new Pcs with enhanced activity. Pcs and their aza analogs, tetrapyrazinoporphyrazines (TPyzPzs), with different central metals bearing either quaternized or non-quaternized triazoles were included in this study to evaluate the effects of the macrocyclic core, central metal and quaternization on photophysical properties and photodynamic activity. The bulkiness of the peripheral 2,6-bis((1*H*-1,2,4-triazol-1-yl)methyl)-4-methylphenoxy substituents was expected to place the triazoles (quaternized or not) above and below the plane of the core. Steric hindrance makes the substituents very rigid; thus, the triazoles cannot bend out of their position and should efficiently protect the core from undesirable aggregation.

RESULTS AND DISCUSSION

Synthesis. The synthetic routes for the target Pc (**6-10**) and TPyzPz (**11-16**) macrocycles bearing eight sterically hindered peripheral phenoxy substituents are shown in Scheme 1. The reaction pathway was started by the synthesis of phenol **1** by the condensation of triazole with 2,6-bis(hydroxymethyl)-4-methylphenol following a previously reported procedure.[18] The initial phthalonitrile **2** and pyrazine-2,3-dicarbonitrile **3** were prepared in good yields from an aromatic nucleophilic substitution reaction between 4,5-dichlorophthalonitrile or 5,6-dichloropyrazine-2,3-dicarbonitrile, respectively, and triazole-containing phenol **1**. To further support the structural identification of the targeted quaternized complexes, quaternized precursors **4** and **5** were prepared from the reaction of **2** or **3** with methyl iodide in DMF at 80 °C.

Scheme 1. Synthetic routes of the studied compounds and their quaternized derivatives[a]

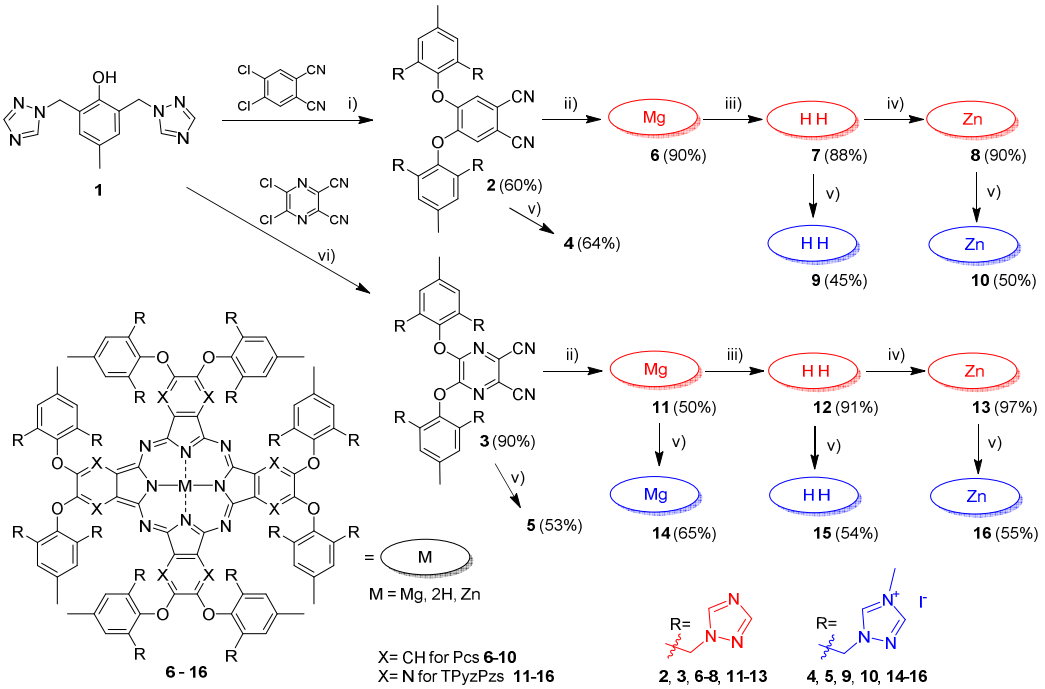

[a]Reagents and conditions: i) CsF, DMF, 80 °C, 24 h; ii) $Mg(OBu)_2$, BuOH, I_2, reflux, 3 h; iii) TsOH, THF, rt, overnight; iv) anhydrous $Zn(OAc)_2$, pyridine, reflux, 3 h; v) DMF, CH_3I, 80 °C, 24 h; vi) acetone, pyridine, rt, 24 h.

The initial attempts to prepare the proposed metal-free Pc and TPyzPz macrocycles using lithium as an initiator in pentanol (*i.e.,* the Linstead method)[20] failed and gave unidentified brown products instead. A metal-ion-mediated cyclotetramerization procedure was successfully used to prepare zinc TPyzPz **13** by the reaction of **3** with anhydrous zinc acetate in dry quinoline under a nitrogen atmosphere, although it gave a very low yield (≤10%). In contrast, magnesium butoxide-induced cyclotetramerization gave Mg complexes **6** and **11** in high yields of 90% and 50%, respectively.[21] Subsequently, demetallation of Mg complexes using *p*-toluenesulfonic acid (TsOH) gave metal-free ligands **7** and **12**, which, in turn, were complexed with a

zinc cation using zinc acetate in pyridine to yield Zn complexes of Pc and TPyzPz **8** and **13**. Both demetallation and zinc complexation proceeded in high yields, typically over 90%. Subsequently, all these Pcs and TPyzPzs were quaternized with methyl iodide to give completely water-soluble quaternized derivatives **9**, **10**, and **14-16**. Notably, the preparation of the quaternized Mg complex of Pc **6** failed using the aforementioned conditions, and the reaction instead gave only the quaternized metal-free Pc **9**. Other attempts using different procedures (in chloroform or DMF at room temperature) also failed. All the synthesized complexes were fully characterized by elemental analysis, IR, ^{1}H NMR and ^{13}C NMR. Elemental and X-ray analyses showed a variable number of water molecules coordinated to the triazole moieties in all of the synthesized complexes, similar to a previous report.[22]

The intrinsic aggregation behavior of the Pcs and their analogs represent the primary obstacle for researchers due to the efficiency limitation of using these materials in PDT applications. Therefore, UV-Vis (see below) and ^{1}H NMR spectroscopic techniques were employed to evaluate the aggregation behavior of the prepared complexes in either organic solvents or water. The ^{1}H NMR spectra of all the prepared complexes were recorded primarily in deuterated DMSO and gave well-resolved spectra with sharp peaks in both the aromatic and aliphatic regions (Supporting Information, Figures S3, S4, S9 and S10). No broadening or peak shifts were observed over a broad concentration range, and the high quality of the spectra remained unchanged with well-resolved peaks, even at high concentrations (ranging from 3–20 mM), indicating the absence of aggregation. In addition, the spectra of both starting precursors **2** and **3** and their corresponding complexes were almost identical and showed exactly the same excellent quality. The metal-free ligands **7**, **9**,

12 and **15** also showed inner core protons that exhibited no chemical shifts at variable concentrations.

Since the prepared polycationic complexes (**9, 10** and **14-16**) were all well soluble in water, their aggregation behavior in an aqueous medium was evaluated by recording their ^{1}H NMR spectra in D_2O. The excellent quality of the NMR spectra obtained in D_2O was similar in terms of features (*i.e.,* well-resolved and sharp peaks) to those obtained in DMSO for the same complexes, as well as to those of the corresponding quaternized precursors **4** and **5**, apart from the chemical shifts resulting from the solvent effect (Supporting Information, Figures S9 and S10). These findings suggested that the aggregation behavior was totally absent in water and thus implied that promising results could be achieved in terms of the photodynamic activity. Notably, the chemical shift for the more acidic proton of the triazole moiety was missing due to D_2O exchange. The ^{13}C APT spectrum of **10** confirmed that the triazole proton had been exchanged with a D atom because the signal appeared as a triplet in the even carbon phase with J = 33 Hz (Supporting Information, Figure S12).

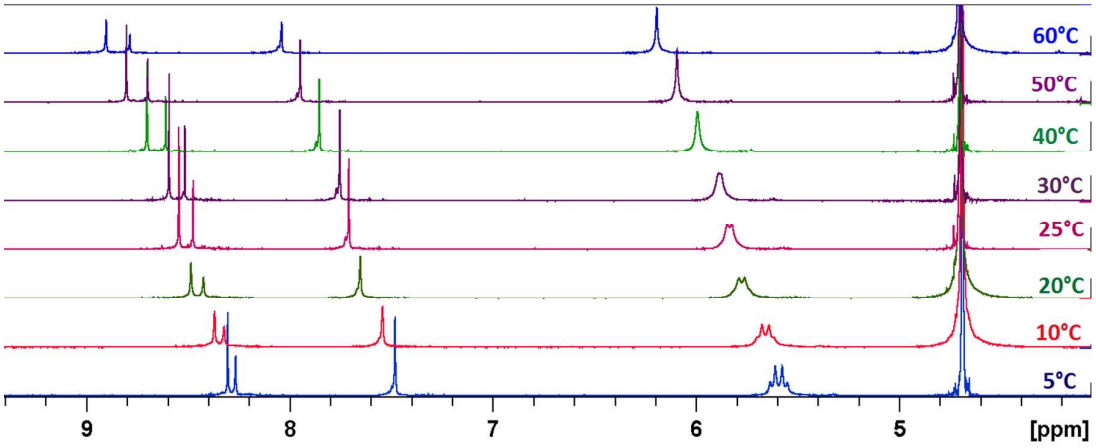

Figure 1. ^{1}H NMR spectra of **10** at variable temperatures from 5 to 60 °C in D_2O.

Interestingly, the two aliphatic protons belonging to methylene groups in complexes **9** and **10** were surprisingly not magnetically equivalent and displayed doublet-of-

doublet resonances with J = 15 Hz in D_2O (not in DMSO, Supporting Information Figure S14), as shown in Figure 1 and Supporting Information, Figure S13. The coupling constant of 15 Hz indicated geminal coupling between the two protons (H-C-H), consequently suggesting the existence of diastereotopic protons. This result could be explained by the presence of a nearby chiral center, presumably the sp^3 nitrogen of the triazole moiety, due to the greatly reduced dynamic of the nitrogen lone pair as a result of the solvent effect and the high rigidity of the complexes themselves. Therefore, variable-temperature studies (5-60 °C) were performed and showed that the coalescence of the methylene peaks (*i.e.,* they became a single peak) in complexes **9** and **10** occurred at 50 °C (Figure 1 and Supporting Information, Figures S13 and S14). The conventional explanation could be related to the loss of N chirality due to the increase in the kinetic energy of its lone pair at higher temperatures. As revealed by the temperature-dependent ^1H NMR spectra (Figure 1 and Supporting Information, Figures S13 and S14), the excellent quality, including the sharp and well-resolved peaks, remained unchanged; the aromatic peaks shifted only slightly into the high-field region.

X-ray single-crystal structures. The unique structural features of the triazole-substituted Pc and TPyzPz analogs were confirmed by single-crystal X-ray diffraction analysis. This technique helped to verify the relative orientations of the various triazole moieties or their quaternized counterparts with respect to the macrocycle ring in the solid state, and it provided valuable information regarding their aggregation behavior and intermolecular interactions. The crystal structures of both triazole-substituted phenoxy phthalonitrile and the corresponding pyrazine precursors **2-5** were also generated (by solvent diffusion techniques) and compared to those of the novel, structurally modified Pcs and TPyzPzs. The crystal structures (Supporting

Information, Figures S33-S36) of these starting compounds confirmed that the plane of the phenoxy rings containing the triazole or methyl triazole moieties was projected almost perpendicular to the aromatic plane containing the nitrile groups and that the rotation of the phenoxy moieties was completely blocked by the presence of bulky substituents.

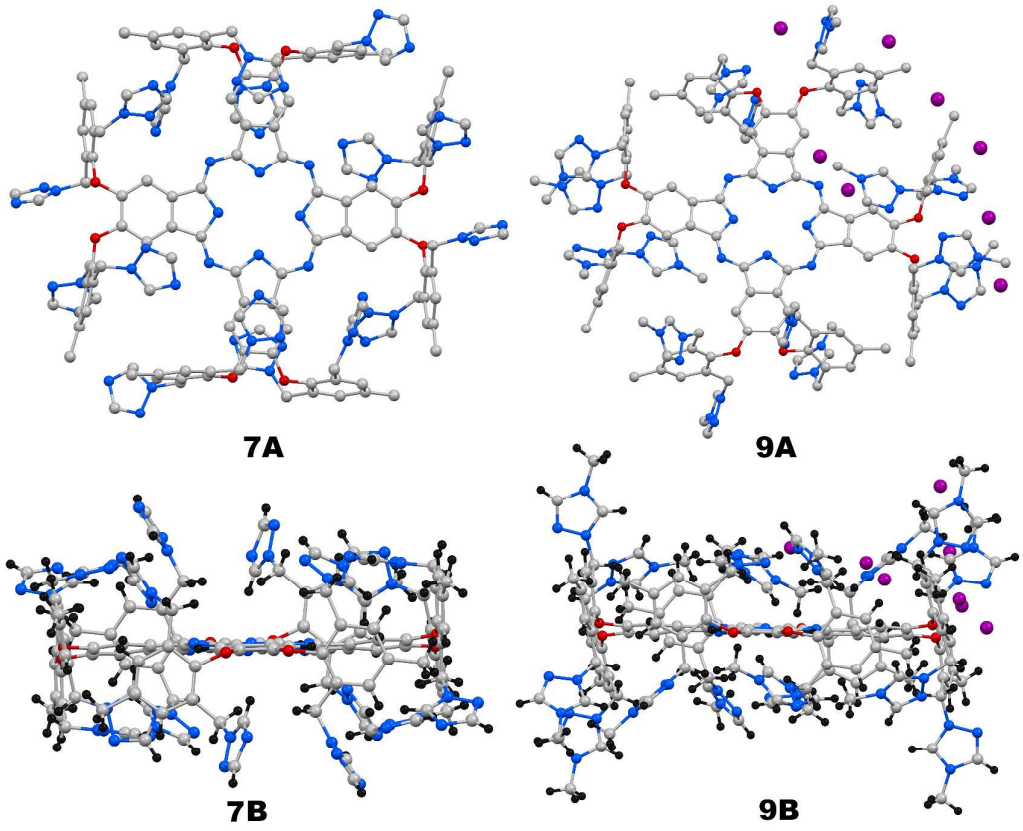

Figure 2. Crystal structures of **7** (7A: top view; 7B: side view) and **9** (9A: top view; 9B side view). Color code: gray-carbon, red-oxygen, blue-nitrogen, violet-iodide and black-hydrogen. In the top view, the hydrogen atoms are hidden for clarity.

Many attempts were made to generate good-quality single crystals of the various triazole-substituted Pcs and their corresponding TPyzPz derivatives. Metal-free Pc **7** and its quaternized analog **9** as well as the Mg and Zn complexes of TPyzPzs **11** and **13** were crystallized in good quality for diffraction analysis. The molecular structures

of these four Pc systems obtained from X-ray diffraction analysis are depicted in Figures 2 and 3. Similar to most of their metal-free analogs,[23] the cores of both **7** and **9** were observed to be planar in their crystal structures. At the same time, the magnesium and zinc ions in **11** and **13** were both positioned slightly above the plane of the corresponding TPyzPz units, and one water molecule was observed to be coordinated to the core metal. As a result, both **11** and **13** had domed shapes with coordinated water at the apex position. The magnesium ion and its coordinated water molecule in **11** exhibited positional disorder and appeared on both sides of the Pc plane. Both of these Mg-H_2O fractions were found to possess half occupancies each; hence, the overall Mg-H_2O occupancy was unity.

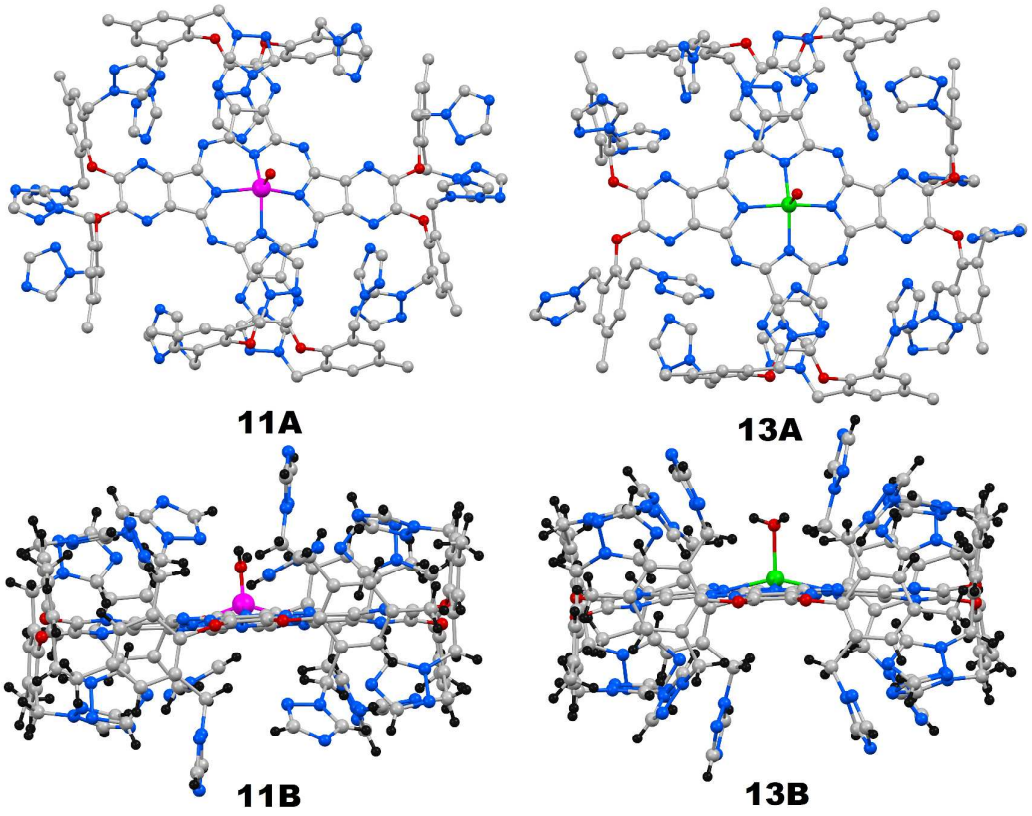

Figure 3. Crystal structures of **11** (11A: top view; 11B: side view) and **13** (13A: top view; 13B side view). Color code: gray-carbon, red-oxygen, blue-nitrogen, pink-magnesium, green-zinc and black-hydrogen. In the top view, the hydrogen atoms are hidden for clarity. In the case of **11**, the occupancy of Mg-H_2O at the opposite side due to positional disorder is hidden.

Similar to the case of precursors **2** and **3**, the peripheral phenoxy units of all these Pcs and TPyzPzs were positioned orthogonally with respect to the plane of the Pc ring. The triazole functional units, which were present at the *ortho* positions of the phenoxy moieties in all of these crystals, were thus oriented just above or below the Pc plane, as depicted in Figures 2 and 3 (all hydrogen atoms and solvent molecules are hidden for clarity). However, their relative orientations with respect to the macromolecular plane were found to be slightly different in each type of crystal, presumably due to steric reasons. This phenomenon was more evident in the case of **9**, where most of the triazole moieties were projected outward from the macrocycle ring. The positioning of triazole moieties either upward or downward with respect to the Pc planes, as revealed from the crystal structures, clearly dismissed the possibility of any face-to-face Pc aggregation among these moieties. The distances (core-to-core) between two Pc or TPyzPz molecules in all these crystal networks were observed to be greater than 10 Å, which was too far away to cause any appreciable face-to-face π-stacking. Additionally, in the case of crystals of **11** and **13**, the phenoxy units orthogonal to the TPyzPz plane were capable of engaging in intermolecular π-π interactions with the adjacent phenoxy fragment of the neighboring TPyzPz units. Moreover, some triazole substituents in the crystal networks that were positioned above or below the ring could also engage in intramolecular π-π interactions with the TPyzPz macrocycle or in intermolecular triazole-triazole π-bonding between adjacent

TPyzPzs. Figure 4 illustrates all such π-π interactions that were observed in the case of the crystals of **11**. In the case of **7**, such triazole-mediated π-bonding was very limited, and these interactions were not observed at all for **9**. Although good-quality single crystals could not be obtained from the other studied Pcs and TPyzPzs to verify their structural features, we could presume that these complexes would also adopt the same orthogonal orientation to effectively avoid cofacial self-association.

Transmission electron microscopy was used to observe morphology of the compounds (Supporting Information, Figure S41). The images revealed that the non-quaternized Pcs **7** and **8** are cubic in shape. After quaternization, the morphology of complexes **9** and **10** converted to the perfect spherical with very narrow size distribution.

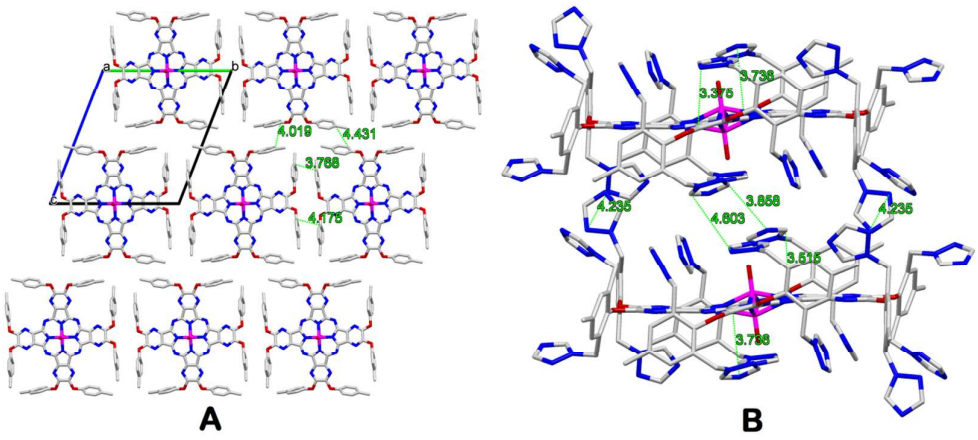

Figure 4. Packing pattern of molecules of **11** in their crystal network showing the possibility of π-π interactions among the adjacent molecules. A: possible π-π interactions of adjacent phenoxy moieties. B: π-π interactions (both intramolecular and intermolecular) among triazole substituents. Hydrogen atoms are hidden for clarity.

Absorption spectra. The UV-Vis spectroscopic technique was used to assess the absorption spectra and further evaluate the aggregation behavior in either organic or

aqueous media. As anticipated, a sharp, unperturbed single Q-band, typical of monomeric Pcs and TPyzPzs with D_{4h} symmetry, was the characteristic feature of all the synthesized metal-containing complexes in DMF (Figure 5 and Supporting Information, Figures S15-S18). The absorption spectra of metal-free ligands **7**, **9**, **12** and **15** were slightly complicated by the full or partial deprotonation of the central NH and will be discussed below. Since the position of the Q-band represents an essential factor for excitation in PDT, we should indicate that the Q-bands of the prepared complexes were located above 678 nm for the Pcs and 630 nm for the TPyzPzs (Table 1). The blue shift of the Q-bands of the TPyzPzs by approximately 50 nm compared with the corresponding Pc derivatives was in good agreement with previously observed trends for these types of dyes.[24] This result makes the Pc derivatives more suitable for application in PDT since light of longer wavelengths typically penetrates more deeply into human tissues.[3] Further assessment was performed to confirm the absence of aggregation by recording the absorption spectra in DMF for each derivative at different concentrations ranging from 1 to 9 μM. As expected, there were no spectral changes as the concentration increased, and the monomeric characteristics were the prominent features for all the inspected complexes, which obeyed the Beer-Lambert law in the studied concentration range (Supporting Information, Figures S15-S17). Furthermore, the solutions were strongly fluorescent (Table 1).

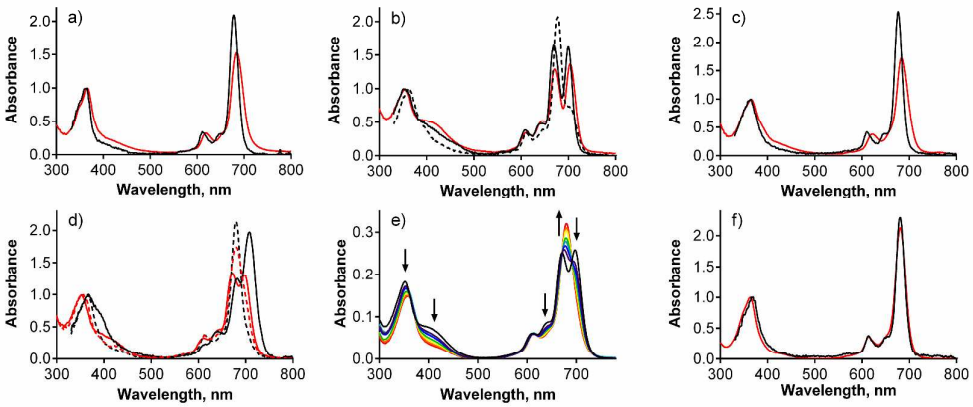

Figure 5. Absorption spectra of the studied Pc derivatives in DMF (black) and in cell culture medium (red) at a concentration of 1 μM. Spectra were normalized to the same absorption in the B-band. Dashed lines represent spectra collected 1 h after sample preparation. A) **6**, B) **7**, C) **8**, D) **9**, E) time-lapse spectral changes of **9** in cell culture medium over 3 h, F) **10**. Samples of water-insoluble compounds **6**-**8** in cell culture medium were prepared from a 300 μM DMF stock solution.

The photophysical properties of PSs can be greatly affected by their aggregation behavior in water or cell culture medium and consequently may determine their activity in PDT applications. All the tested compounds (**6**-**16**) (the solutions of the non-quaternized derivatives were prepared from a DMF stock solution) displayed absorption spectra in water or in cell culture medium that were typical of predominantly monomeric species. While the Q-band of the quaternized derivatives was sharp (sometimes even sharper than in DMF) and the solutions exerted strong fluorescence, the spectra of the non-quaternized derivatives were slightly broader, and the Q-band was less intense (Figures 5 and S18) and was accompanied by a loss of fluorescence, with Φ_F typically below 0.01 in water (Table 1). These data suggested that the polycationic species remained fully non-aggregated in water-based media, while atypical types of aggregates with absorption spectra with a predominantly

monomeric character were observed for the non-quaternized derivatives in water, similar to previous results for hydrophilic Pcs and TPyzPzs with extremely bulky substituents.[25] We believed that these aggregates could be formed based on the intermolecular π-π interactions between phenoxy substituents and/or triazole units that were observed in the crystal structure of non-quaternized **11** (Figure 4). No such interactions were observed in quaternized **9**. At the same time, the distance between the Pc cores in **11** (more than 10 Å) was not sufficient for face-to-face aggregation (which would change absorption spectra), as indicated by the crystal structure. However, this distance was within the range of energy resonance transfer between two Pc molecules, which could deactivate the excited state without changing the absorption spectra. Although we are aware that the situation in water can be different from that in the solid state in crystal, the presence of such intermolecular interactions seems to be a plausible explanation.

The Q-band absorption maxima (*i.e.,* shape and position) of the polycationic compounds in water were independent of concentration and followed the Beer-Lambert law with a constant extinction coefficient in the studied concentration range (1 to 9 μM, Supporting Information, Figures S16 and S17). Additionally, the UV-Vis spectra of Zn complexes **10** and **16** were assessed under different conditions. The shape of the Q-band remained fully constant (Supporting Information, Figure S19), with strong fluorescence of the solutions in water, in buffers with pH values of 2, 7, and 11, and in cell culture medium at a concentration up to 120 μM, suggesting that there was no effect of dye concentration, pH, ion concentrations or serum proteins on the monomeric character of these species. The absence of aggregation in aqueous solution exhibited by the prepared polycationic complexes appeared to be intrinsically related to the orthogonal conformation adopted by the eight peripheral bulky phenoxy

substituents, as clearly demonstrated in the single-crystal X-ray structures (Figure 2). The quaternized nitrogens formed two "cationic donuts" of positive charges that efficiently protected the hydrophobic core from cofacial interactions by electrostatic repulsive forces. This excellent monomeric character in water under different conditions is extremely rare in Pcs and TPyzPzs and is a valuable prerequisite for high photodynamic activity.

As briefly mentioned above, metal-free ligands **7**, **9**, **12** and **15** exhibited atypical behavior in that they were deprotonated at the acidic central NH.[26] The Q-bands of **7** and **12** remained typically split due to the reduced D_{2h} symmetry (Supporting Information, Figure S20) in non-basic organic solvents (THF and $CHCl_3$). However, the deprotonation of the central NH in DMF or pyridine restored (sometimes only partially) the D_{4h} symmetry of the macrocycle, and the Q-band was found to be single and unsplit. TPyzPzs are typically more acidic,[27] which was why the absorption spectra of both **12** and **15** were predominantly deprotonated shortly after dissolution in DMF, water or cell culture medium (Figure 6). In the case of Pcs **7** and **9**, the splitting was observed in DMF, water and cell culture medium shortly after dissolution, although the spectrum gradually changed with time, reaching the fully deprotonated form approximately 3 h after dissolution in one experiment (Figure 5 C, D, F). Notably, the extent and rate of NH deprotonation changed from batch to batch, which meant that it could not be properly characterized.

Table 1. Photophysical data for the target complexes in DMF and water.[a]

Cpd.	λ_{max} (log ε) DMF	λ_{max} (log ε) water	Φ_F[b] DMF	Φ_F[b] water	λ_F DMF	λ_F water	τ_F / ns DMF	τ_F / ns water	Φ_Δ[b] DMF	$\Phi_\Delta + \Phi_F$ DMF
6	679 (5.31)	-	0.537	0.011	685	689	5.57	-	0.224	0.760
7	669 (5.13), 700 (4.95)	-	0.276	0.005	705	708	4.78	-	0.258	0.534
8	678 (5.41)	-	0.269	0.0025	684	700	2.81	-	0.588	0.857
9	677 (5.33)[c]	670 (5.08), 697 (5.03)	0.230[c]	0.157	686[c]	706	2.33 (33%), 4.91 (67%)	1.09 (26%), 3.70 (74%) (1.50)	0.270	0.500
10	680 (5.33)	681 (5.49)	0.146	0.187	687	690	1.68 (17%), 2.89 (83%)	1.22 (6%), 2.76 (94%) (1.19)	0.478	0.625
11	630 (5.12)	-	0.349	0.010	637	637	1.07 (4%), 4.51 (96%)	-	0.336	0.685
12	630 (5.11)[c]	-	0.142[c]	0.011	638[c]	655	1.30 (35%), 2.69 (65%)	-	0.420	0.562
13	632 (5.16)	-	0.162	0.0055	636	636	1.18 (19%), 2.26 (81%)	-	0.600	0.761
14	633 (5.22)	638 (5.00)	0.074	0.216	664	651	1.20 (8%), 4.82 (92%)	1.18 (3%), 5.09 (97%)	0.082	0.156
15	632 (4.90)[c]	633 (5.31)[c]	0.071	0.028	638[c]	660[c]	0.93 (20%), 3.47 (80%)	0.56 (38%), 2.63 (62%)	0.091	0.162
16	634 (5.20)	643 (4.95)	0.033	0.124	657	647	0.96 (13%), 2.26 (87%)	0.80 (4%), 2.71 (96%)	0.137	0.170

[a]Q-band absorption maximum (λ_{max}); extinction coefficient (ε); emission maximum (λ_F); fluorescence lifetime (τ_F); fluorescence quantum yield (Φ_F); singlet oxygen quantum yield (Φ_Δ). [b]Unsubstituted ZnPc was used as the reference compound (Φ_Δ = 0.56 in DMF[28], Φ_F = 0.32 in THF[21]). [c]Predominantly deprotonated species.

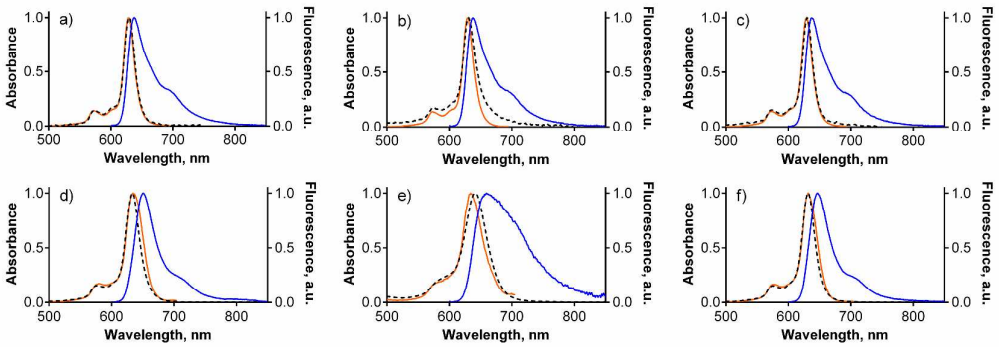

Figure 6. Normalized absorption (black, dashed), excitation (orange) and emission (blue) spectra in DMF (A-C) and water (D-F) of the studied TPyzPzs: A) **11**, B) **12**, C) **13**, D) **14**, E) **15**, and F) **16**.

Photophysical characterization. Singlet oxygen is believed to be the primary cytotoxic species in PDT, and fluorescence emission is often used to localize PSs at the subcellular level or in animal and human tissues. The quantum yield of singlet oxygen (Φ_Δ), quantum yield of fluorescence (Φ_F) and fluorescence lifetimes (τ_F) were therefore determined in DMF and in water (for fluorescence) by the comparative method using unsubstituted zinc phthalocyanine (ZnPc) as the reference compound. The photophysical data are summarized in Table 1. The results in Table 1 were in good agreement with previously published data in terms of the presence of a central metal and its heavy-atom effect.[29] The zinc complexes of these particular ligands were always stronger producers of singlet oxygen, while the magnesium complexes exhibited much stronger fluorescence. The properties of the metal-free ligands could not be properly compared to the others because of different levels of deprotonation during measurement and because both forms (protonated and deprotonated) may exhibit different photophysical behaviors.[30] Nevertheless, it seemed that both singlet oxygen production and fluorescence were reduced in these derivatives, in agreement with previous observations of similar metal-free Pcs and TPyzPzs.[21] Interestingly,

both quantum yields of the polycationic TPyzPzs (**14-16**) in DMF were substantially lowered, as seen from the sum of these most important relaxation pathways of the excited state (Table 1). However, their Φ_F values in water were substantially increased. At the same time, the fluorescence decays were best characterized by two lifetimes for compounds **14-16** but also for **9-15**. This fact could indicate the induction of some non-radiative relaxation pathway (most likely photoinduced electron transfer between deprotonized acidic CH in triazole and macrocyclic core) and may be of interest in future research.

As briefly mentioned above, the polycationic compounds were monomeric in aqueous solution. This observation was accompanied by comparable or even greater Φ_F values in water media than in DMF, further emphasizing their monomeric character. On the other hand, the non-quaternized derivatives, despite their seemingly monomeric absorption spectra, were almost non-fluorescent in water (Φ_F typically $\leq$0.01), indicating that they were losing their photodynamic potential. Their fluorescence was slightly improved (typically by up to 3-fold, data not shown) upon dissolution in cell culture medium, which suggested interactions with serum (lipo)proteins and separation of the molecules. This result was further confirmed by the titration of selected compounds with fetal bovine serum (FBS, see below).

The emission spectra of all the studied Pcs and TPyzPzs were typically mirror images of the Q-band and were characterized by a small Stokes shift. The excitation spectra of the metal complexes were in perfect agreement with the absorption spectra, even for the polycationic compounds in water media, further confirming the presence of monomeric species in solution (Figure 6 and Supporting Information, Figure S21). In the case of the metal-free ligands, the excitation spectra sometimes did not perfectly match the absorption spectra due to the different levels of deprotonation and

the apparently different photophysical (*i.e.,* fluorescence) properties of the protonated and deprotonated species. Specifically, in the spectra of metal-free Pc **9** in water, the Q-band in the absorption spectrum indicated the presence of the predominantly protonated form, while the excitation spectrum suggested the presence of the prevalently deprotonated form, which seemed to be the more fluorescent species in solution (Supporting Information, Figure S21).

Log *P*. Lipophilicity, expressed as log *P* (*P* is the partition coefficient between octanol and water), is an important parameter for drugs. The log *P* values for the studied Pcs and TPyzPzs were determined experimentally (Table 2). Quaternized compounds **9**, **10**, and **14**-**16** were detected primarily (or exclusively in the case of **10;** no signal was detected in octanol) in the water phase because of their polycationic character. The non-quaternized triazoles in **6** and **8** did not make the compounds very hydrophilic, and they were found preferentially in the octanol phase. Log *P* could not be determined for some of the non-quaternized derivatives (**7** and **11**-**13**) since they precipitated in the interphase, and the amounts detected in each phase were not significant.

Table 2. Comparison of the log *P*, dark toxicity (TC_{50} values), and photodynamic activity (EC_{50} values) of the studied PSs in different cell lines.[a]

Cpd.	log *P*	EC_{50} (μM)				TC_{50} (μM)		TC_{50}/EC_{50}	
		HeLa	MCF-7	HCT 116	HaCaT	HeLa	HaCaT	HeLa	HaCaT
6	1.34	>1[b]	>1[b]	>1[b]	>1[b]	>1[b]	>1[b]	n/a	n/a
7	n/a[c]	>1[b]	>1[b]	>1[b]	>1[b]	>1[b]	>1[b]	n/a	n/a
8	0.35	0.53 ± 0.099	0.44 ± 0.011	0.64 ± 0.038	0.61 ± 0.027	>1[b]	>1[b]	>2	>2
9	-0.77	0.042 ± 0.016	0.051 ± 0.028	0.15 ± 0.061	0.081 ± 0.006	276 ± 21	550 ± 22	6571	6790
10	<-3.0[d]	0.012 ± 0.004	0.0053 ± 0.0008	0.0087 ± 0.0002	0.0065 ± 0.0013	369 ± 53	874 ± 20	30750	134500
11	n/a[c]	>1[b]	>1[b]	>1[b]	>1[b]	>1[b]	>1[b]	n/a	n/a
12	n/a[c]	>1[b]	>1[b]	>1[b]	>1[b]	>1[b]	>1[b]	n/a	n/a
13	n/a[c]	>1[b]	>1[b]	>1[b]	>1[b]	>1[b]	>1[b]	n/a	n/a
14	-2.00	1.18[e]	22.4[e]	3.16[e]	2.71[e]	433 ± 24	1081 ± 125	367[e]	400[e]
15	-1.53	>100	>100	>100	>100	363 ± 27	979 ± 44	n/a	n/a
16	-1.53	0.064 ± 0.013	0.038 ± 0.004	0.039 ± 0.003	0.026 ± 0.0012	436 ± 44	637 ± 28	6813	24500
verteporfin[f]	1.56	0.036 ± 0.010				18.6 ± 4.2		510	
temoporfin[f]	1.15	0.045 ± 0.007				20.6 ± 2.5		460	
Pp IX[f]	0.06	0.80 ± 0.13				>10		>10	

S_3AlOHPc[f]	-2.12	2.07 ± 0.29	127 ± 7.8	60

[a]Data are presented as the TC_{50} or EC_{50} values ± standard deviations. Irradiation conditions: $\lambda > 570$ nm, 12.4 mW cm^{-2}, 15 min, 11.2 J cm^{-2}. [b]The compounds precipitated at concentrations above the listed values. [c]Compound precipitated during determination. [d]Compound detected only in water phase. [e]Ambiguous data (viability decreased only approx. up to 50% and then remained constant up to a concentration of 50 μM; 100% decrease in viability was not obtained). [f]Data from ref.[19]

***In vitro* evaluation of dark toxicity and photodynamic activity**. Promising photophysical data with high singlet oxygen production for the zinc complexes and excellent water solubility with a fully monomeric character in water, even at high concentrations, for polycationic macrocycles are valuable prerequisites for potentially successful PSs. All Pcs and TPyzPzs were therefore evaluated (Table 2) for their photodynamic activity after irradiation (λ > 570 nm, 11.2 J cm^{-2}, expressed as the half-maximal effective concentration, EC_{50}) in human cervical carcinoma (HeLa), human breast carcinoma (MCF-7), and colorectal carcinoma (HCT 116) cell lines as well as human keratinocytes (HaCaT). Inherent toxicity without activation (expressed as the half-maximal toxic concentration, TC_{50}) was assessed in HeLa and HaCaT cells as representatives of cancerous and normal cell lines, respectively. Stock solutions of the polycationic compounds (**9**, **10** and **14**-**16**) were prepared in cell culture medium without any additives, while the non-quaternized derivatives (**6**-**8** and **11**-**13**) were prepared in DMSO and diluted to the required concentration with cell culture medium.

The inherent toxicity of polycationic Pcs **9** and **10** and TPyzPzs **14**-**16** without activation was very low, with TC_{50} values typically greater than 300 μM (Table 2, Figure 7 and Supporting Information, Figure S22) in HeLa cells; TPyzPzs were slightly less toxic than Pcs. This low toxicity seems to be a general property of similarly substituted Pcs and TPyzPzs.[18,19] The other apparent difference arose from the obviously lower toxicity against normal (HaCaT) cells compared with that against cancerous (HeLa) cells: the TC_{50} values were greater 500 μM, at times reaching even millimolar concentrations (Table 2 and Supporting Information, Figure S23). Routine phase-contrast microscopy observation of the cells during treatment revealed that non-

quaternized compounds **6-8** and **11-13** precipitated from the solution at micromolar concentrations, which was why their TC_{50} values could not be determined.

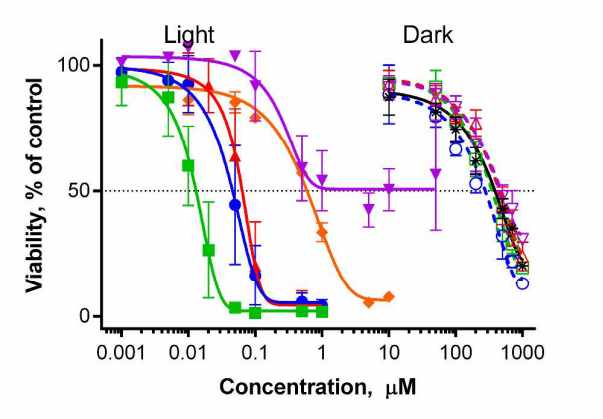

Figure 7. Photodynamic activity (λ > 570 nm, 12.4 mW cm^{-2}, 15 min, 11.2 J cm^{-2}; full lines and full symbols) and dark toxicity (dashed lines and open symbols) in HeLa cells of **8** (orange, rhombus), **9** (blue, circle), **10** (green, square), **14** (magenta, reverse triangle), **15** (black, asterisk) and **16** (red, triangle). At least five independent experiments, each in quadruplicate, were typically performed.

After activation by light, some of the compounds induced a lethal photodynamic effect on the cells (Figure 7 and Supporting Information, Figures S22 and S23). Very high activity was observed for polycationic **9**, **10** and **16** in all tested cell lines with low EC_{50} values. The most susceptible cell line to PDT treatment seemed to be MCF-7, which generally had the lowest EC_{50} values for all the active compounds. No significant difference was detected between the cancerous and normal cell lines, indicating the rather nonspecific effect of singlet oxygen on the cells. Selectivity in PDT *in vivo* is, however, achieved by the irradiation of the selected area only. Considering the structure-activity relationships, the Zn complex of cationic Pc **10** appeared to be extraordinary active, with better activity than structurally similar hexadeca-cationic ZnPc with quaternized imidazolyl moieties (EC_{50} = 37 nM, HeLa,

λ > 570 nm, 11.2 J cm^{-2}),[18] followed by zinc TPyzPz **16** and metal-free Pc **9**, thus indicating superior performance of the zinc complexes and Pc core over the TPyzPz core and other central metals. Unusual behavior following the photodynamic treatment was observed for polycationic magnesium TPyzPz **14**. Viability decreased in a concentration-dependent manner (Figure 7 and Supporting Information, Figures S22 and S23), reaching approximately 50% viability and then remaining at this level, even at high concentrations (50 μM). Currently, we do not have a clear explanation for this atypical result, which was obtained in all tested cell lines. The cationic charges on the triazoles seemed to be crucial for efficient photodynamic activity. With exception of Zn complex of Pc **8** with rather modest activity (EC_{50} ~ 0.50 μM), no photodynamic effect on HeLa cells was observed for the non-quaternized derivatives **6**, **7**, and **11**-**13** up to the maximum possible tested concentration. The most likely explanation for the low activity of these derivatives was the aforementioned formation of aggregates in water and cell culture medium, which did not occur for the cationic derivatives.

Evaluations of the photodynamic activity of novel PSs are always hampered by low transferability of the published results. The different cell lines, light sources and irradiation conditions used by different research groups make comparisons of their results difficult. For this reason, we recently assessed four clinically approved PSs (verteporfin,[31] temoporfin,[32] protoporphyrin IX (Pp IX)[33] and S_3AlOHPc[6]) under the same conditions utilized in this study.[19] As seen from the photodynamic results listed in Table 2, the obtained polycationic compounds performed comparably (**9** and **16**) or even much better (**10**) than the best clinically approved PSs tested under our conditions. Additionally, the Pcs and TPyzPzs were at least an order of magnitude less toxic without activation, and the "therapeutic ratio" (TC_{50}/EC_{50}) for the most

promising compound (**10**) was approximately two orders of magnitude better than the ratios for verteporfin and temoporfin.

Photodynamic treatment is not only drug-dose dependent; the amount of activation light may also play a significant role. Thus, the EC_{50} values for active compounds **8-10** and **16** in HeLa cells were determined with longer and shorter irradiation times of 30 min and 5 min, which resulted in total fluences of 22.4 J cm^{-2} and 3.7 J cm^{-2}, respectively. With the increased light dose, the EC_{50} values significantly improved to 296 nM, 25 nM, 6 nM and 20 nM for **8-10** and **16**, respectively (Figure 8 and Supporting Information, Figure S22). As expected, a radical decrease in the light dose resulted in a reduction in the photodynamic effectiveness, with increases in EC_{50} values to 702 nM, 269 nM, 32 nM and 71 nM for **8-10** and **16**, respectively (Figure 8 and Supporting Information, Figure S22). This experiment clearly demonstrated that the efficacy of PDT was also a function of the light dose. At the same time, it confirmed the low comparability of published photodynamic results to each other, unless the same irradiation source and conditions are used.

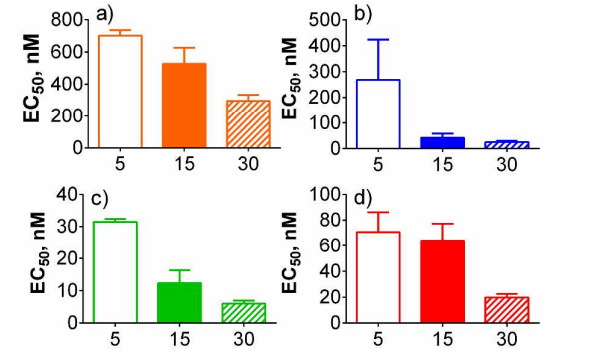

Figure 8. Dependence of EC_{50} values in HeLa cells on irradiation time (in min) for compounds **8** (A, orange), **9** (B, blue), **10** (C, green) and **16** (D, red). The irradiation

conditions were $\lambda > 570$ nm and 12.4 mW cm^{-2}. Irradiation for 5, 15 and 30 min resulted in total fluences of 3.7 J cm^{-2}, 11.2 J cm^{-2} and 22.4 J cm^{-2}, respectively.

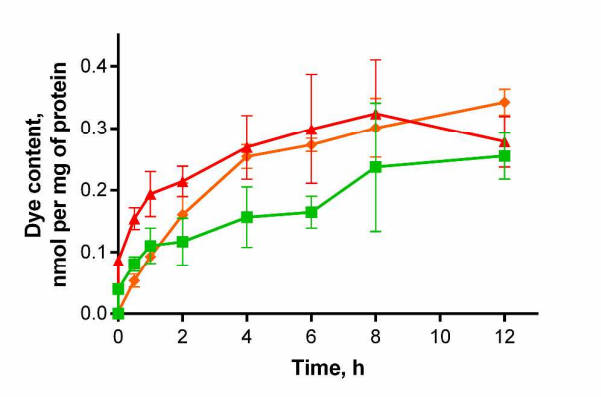

Figure 9. Cellular uptake of compounds **8** (orange, rhombus), **10** (green, square) and **16** (red, triangle) by HeLa cells after incubation with a concentration of 4 μM (for **10** and **16**) or 1 μM (for **8**) of the dye. The experiments were performed in duplicate.

Uptake. The amount of the dye inside the cells could influence the final photodynamic effect. The uptake profiles in HeLa cells were therefore determined for active compounds **8**, **10** and **16**. Metal-free **9** could not be tested due to different amounts of the deprotonated form during testing, which did not allow a determination of the clear dependence of the fluorescence signal on incubation time. As seen from Figure 9, the uptake of all compounds started relatively quickly within the first few hours, reaching a relatively steady level at 12 h, which was used for incubation before photodynamic treatment. The amount of the studied PSs in cells after 12 h was almost the same: 0.26 nmol/mg of protein and 0.28 nmol/mg of protein for cationic derivatives **10** and **16**, respectively. Non-quaternized **8** was taken up by cells to a slightly greater extent (0.34 nmol/mg of protein). Its uptake by cells was most likely even higher since the concentration used for the incubation of HeLa cells with this compound was only 1 μM, while a concentration of 4 μM (used routinely in our

laboratory for these experiments[19,34]) was applied for **10** and **16**. The lower concentration of **8** was used to avoid the possible precipitation of this compound in cell culture medium, which could lead to the misinterpretation of the obtained results.

Subcellular localization. The short lifetime of singlet oxygen is the main reason why the assessment of the subcellular localization of novel compounds is crucial—the position within the cell indicates the primary target of the photodamage induced by PSs. For subcellular localization, specific fluorescent probes for mitochondria (MitoTracker) and lysosomes (LysoTracker) were used, along with the intrinsic fluorescence of the Pcs and TPyzPzs. All of the studied quaternized PSs (**9**, **10** and **14-16**) were detected in the acidic endolysosomal compartment as punctate fluorescence colocalized with the lysosomal probe (Figure 10 and Supporting Information, Figures S25, S27 and S28). For the non-quaternized derivatives (**6-8** and **11-13**), some aggregates were visibly attached to the outside of the cellular membrane (clearly observed as clumps by routine phase-contrast microscopy and by differential interference contrast (DIC) microscopy; Supporting Information, Figures S24 E, K, Q and S26 E, K, Q). No colocalization of these clumps with intracellular organelles was detected by either MitoTracker or LysoTracker. Only the zinc non-quaternized derivatives (**8** and **13**) were detected as punctate fluorescence colocalized with the lysosomal probe (Supporting Information, Figure S24 M and 26 M) in addition to their presence in the clumps.

The localization was further confirmed for the most active Pc **10** by staining with another specific probe (ER-Tracker) together with various organelle-specific protein transfections (Lamp1-RFP for lysosomes,[35] Rab7a-GFP for late endosomes[36] and GALNT2-RFP for the Golgi apparatus[37]) (Figure 10). The punctuate fluorescence of **10** was exclusively colocalized with markers for the endolysosomal compartment

(Lamp1 and Rab7a; Figure 10 E, F). The endoplasmic reticulum typically appeared as a fine tubular network throughout the whole cell that was very dense in the perinuclear area and well resolved in the peripheral parts of the cytoplasm (Figure 10 C, green). The Golgi apparatus, on the other hand, was localized to the perinuclear area only and was characterized by its typical cisternae-like morphology (Figure 10 C, blue). No colocalization with the endoplasmic reticulum or the Golgi apparatus was observed (Figure 10 C, D).

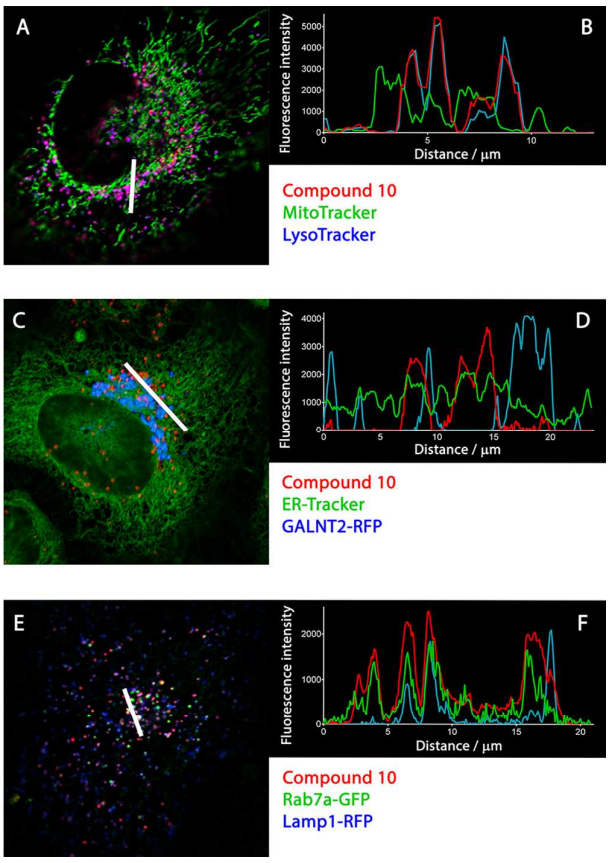

Figure 10. Subcellular localization of compound **10** (red) in HeLa cells. A – MitoTracker (green) and LysoTracker (blue). C – ER-Tracker (green) and GALNT2-RFP (blue). E – Proteins specific for the endolysosomal compartment, Rab7a-GFP (green) and Lamp1-RFP (blue). B, D, F – corresponding fluorescence intensity profiles.

Morphological changes. The primary target of the photodynamic activity of the studied compounds, which were demonstrated to be potent PSs, were the vesicles of the endolysosomal compartment—lysosomes, in particular—which was confirmed by subcellular localization studies. It is likely that activation of PSs leads to damage to the membranes of these organelles, which results in the relocalization of the PSs and damage to other subcellular components. A low dose of **10** (EC_{15} = 4.5 nM) resulted only in the condensation of the ER signal in the perinuclear area in some cases 1 h after irradiation (Supporting Information, Figure S32 N), the simultaneous retraction of some cells (Supporting Information, Figure S32 B) and a slightly lowered amount of cells compared with the control (corresponding to a 15% decrease in viability) 24 h after treatment (Supporting Information, Figure S30 B). Extensive morphological changes were observed with a high dose of **10** (EC_{85} = 25.1 nM) after irradiation (Figure 11 and Supporting Information, Figures S29-32). Retraction from the surface (Supporting Information, Figure S31 C), shortening and rounding of mitochondria (Supporting Information, Figure S31 I), loss of the filamentous ER network (Supporting Information, Figure S31 O), extensive formation of massive membrane protrusions (blebs and blisters; Supporting Information, Figure S29 C and S31 C) filled with homogeneous fluorescence due to the presence of free α-tubulin (Supporting Information, Figure S29 L), relocation of the actin cytoskeleton to the cellular periphery (Supporting Information, Figure S29 I) and chromatin condensation accompanying nuclear shrinkage were detected 1 h after irradiation (Supporting Information, Figures S29 F and S31 L). Heavily damaged and dead cells displayed flat morphology 24 h after treatment (Supporting Information, Figure S32 C), with the loss of the mitochondrial signal (Supporting Information, Figure S32 F) and of the typically filamentous actin and tubulin cytoskeleton (Supporting Information, Figures

S30 I and S30 L) and the shrinking of the nuclei with condensed chromatin (Supporting Information, Figures S30 F and S32 L). The surviving cells, on the other hand, were retracted (Supporting Information, Figure S32 C) but displayed normal, filamentous mitochondrial, ER and nuclear morphology together with preserved microtubules (Supporting Information, Figures S30 C and S32 F). The actin cytoskeleton still appeared to be relocated to the cell periphery, with short spike-like protrusions and a decreased number of stress fibers (Supporting Information, Figure S30 I).

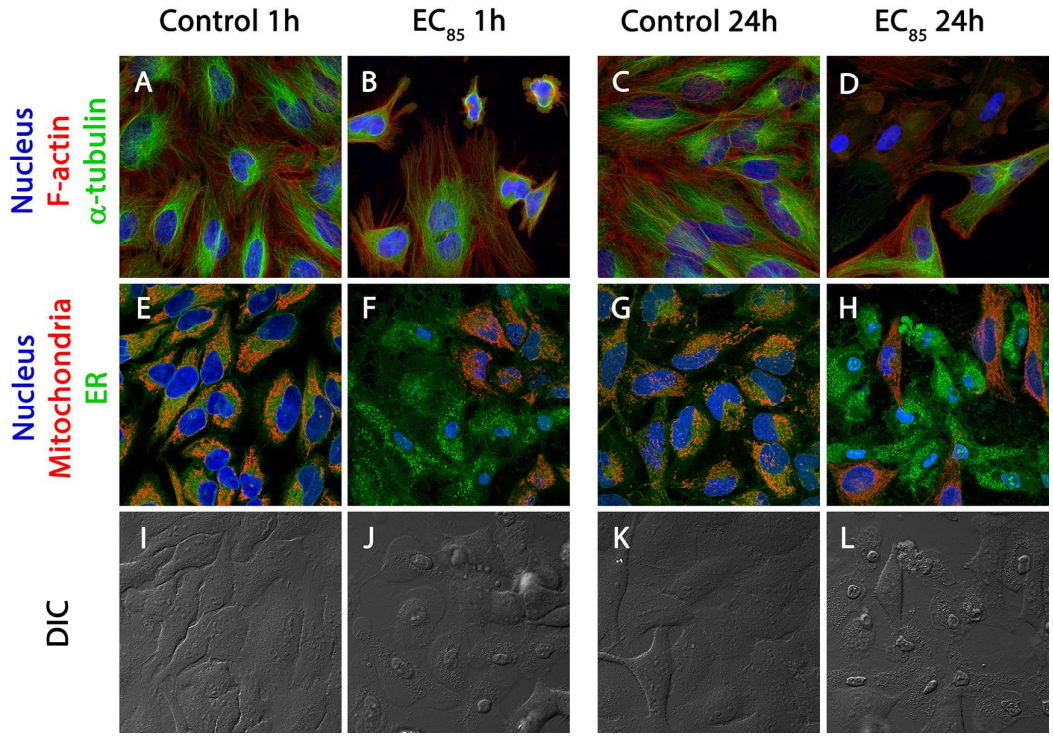

Figure 11. Morphological changes induced by the photodynamic activity of **10**. Changes in general cellular morphology – DIC (I-L), cytoskeleton (A-D, red – actin, green – tubulin), mitochondria (E-H, red), endoplasmic reticulum (E-H, green) and nuclei (A-H, blue).

Flow cytometry. The morphological changes mentioned above indicated severe damage to the cells resulting in irrefragable cell death. To confirm whether this

response occurred *via* programmed cell death (apoptosis, in particular) or *via* accidental cell death (necrosis) as a result of massive oxidative stress, we employed flow cytometry together with propidium iodide (PI) and Annexin V-Alexa Fluor 488 staining. This method was able to distinguish cells (those that were able to preserve their integrity and were not broken down to debris, *e.g.*, by mechanical manipulation) into three populations: non-apoptotic cells (negative for both PI and Annexin), cells undergoing apoptosis (positive for Annexin only) and cells in the late stages of apoptosis or undergoing necrosis (positive for PI). These results suggested that necrotic cell death occurred predominantly, with a significant number of apoptotic cells observed only in cells treated with low dose of **10** and also 24 h after treatment with high dose of **10** (Figure 12).

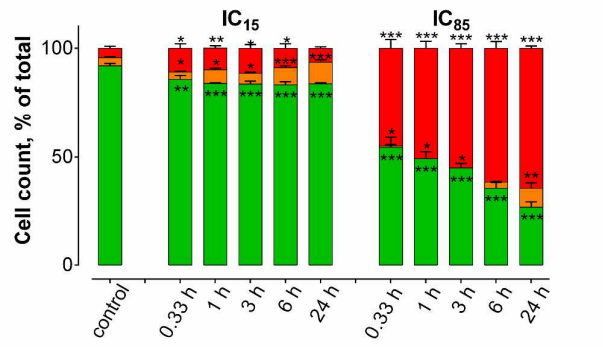

Figure 12. Flow cytometry assessment of HeLa cell death induced by the photodynamic action of **10** analyzed at different times after irradiation (20 min, 1 h, 3 h, 6 h, 24 h) at concentrations corresponding to the EC_{15} and the EC_{85}, expressed as the cell count based on Annexin V−Alexa Fluor 488 and/or PI positivity. Non-apoptotic cells (green), apoptotic cells (orange), and late apoptotic/necrotic cells (red). The experiments were performed in triplicate. *, $p < 0.05$; **, $p < 0.01$; ***, $p < 0.001$.

Interaction with serum proteins. In several cases in the literature, interactions with serum proteins have been shown to influence photodynamic activity both positively[38] and negatively.[34] The interaction of PSs with albumin, the most abundant protein in serum, was also tested as a delivery pathway with increased selectivity for cancer cells.[39] To determine their interactions with serum proteins, the tested compounds (**8**-**10** and **16**) were dissolved in serum-free cell culture medium, and the solutions were titrated with increasing amounts of FBS up to 12% of serum in medium (the typical amount of FBS in cell culture medium is 10%) while their fluorescence signals and absorption spectra were monitored. No significant change in emission band position or Q-band shape was observed up to the maximum tested concentration in the case of polycationic compounds **9**, **10** and **16** (Figure 13). Together with very small decrease in the fluorescence intensity it indicated that no or very limited interactions with serum proteins occurred for these compounds, similar to other multicationic Pcs and analogs reported in the literature.[19,34] However, a significant increase (almost 12-fold) in fluorescence at 10% FBS concentration was detected for non-quaternized Pc **8**. This compound had very low fluorescence (Φ_F < 0.002) in serum-free media as a consequence of the formation of atypical aggregates (see above) in water-based environments. The increase in the fluorescence signal after the addition of FBS indicated the interaction of this Pc with proteins (most likely with their hydrophobic pockets) and the separation of the Pc molecules as well as their activation. However, the activation was apparently not very efficient, as the $\Phi_F \sim 0.02$ in cell culture medium with 10% FBS was still very low and suggested only weak activity (compare to $\Phi_F = 0.27$ for **8** in DMF, where the compound is strictly monomeric). This result was in agreement with the rather modest photodynamic activity (EC_{50} = 0.53 μM, HeLa cells) determined for this compound.

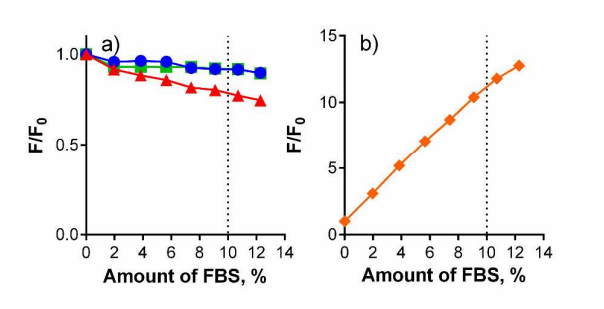

Figure 13. Changes in fluorescence intensity of (A) cationic compounds **9** (blue, circle, λ_{em} = 692 nm), **10** (green, square, λ_{em} = 691 nm), and **16** (red, triangle, λ_{em} = 642 nm) and (B) non-quaternized **8** (orange, rhombus, λ_{em} = 688 nm) after the addition of FBS to the serum-free cell culture medium. The dye concentration was 1 μM. Vertical dashed line indicates the typical amount of FBS in cell culture media.

CONCLUSION

In summary, we reported the synthesis, full characterization and structure-activity relationships of promising PSs from the family of Pcs and TPyzPzs. Peripheral substitution with bulky phenoxy substituents bearing triazole moieties perfectly inhibited the aggregation of the compounds in DMF solution and, for the quaternized derivatives, in water as well, with no influence on the monomeric state of the quaternized compounds from the concentration, pH, ionic strength or presence of serum proteins. As confirmed by X-ray crystallography, this excellent behavior resulted from the specific spatial arrangement of the peripheral phenoxy substituents that adopted an orthogonal orientation. In this orientation, the quaternized triazole moieties were placed rigidly above and below the hydrophobic core, similar to two "cationic donuts", and they effectively protected the core from cofacial self-association. In the case of the non-quaternized derivatives, atypical aggregates with seemingly monomeric absorption spectra and completely non-fluorescent properties were observed in water and cell culture medium, which could be explained by the

intermolecular π-π interactions between the phenoxy and/or triazole units that were found in the crystal structures. Although these aggregates could be partially broken up through interactions with FBS, this effect was not sufficient to provide these compounds with high photodynamic activity. The photodynamic activity was therefore the strongest for the quaternized compounds that were present in an active form in water, even at concentrations far above 100 μM. The strongest photodynamic effect was detected for Pc **10** with EC_{50} = 12 nM in HeLa cells, several times better than the best performing clinically approved PS under the same irradiation conditions. Polycationic compounds **9** and **16** appeared to also be highly active at approximately the same level as the commercial PSs. The potential of Pc **10** in PDT was further increased by its low dark toxicity, effectiveness against other cancerous cell lines and activation by light above 680 nm. All the quaternized compounds and the zinc non-quaternized derivatives were found to be localized to the endolysosomal compartment, as this is the primary target after irradiation. The activation of **10** induced severe morphological changes connected to cellular damage and cell death shortly after irradiation, including cell retraction, membrane protrusion and bleb formation, nuclear shrinkage, and chromatin condensation as well as damage to the mitochondria, ER and cytoskeleton. These morphological traits together with the flow cytometry results suggested the necrotic route of cell death. In conclusion, we demonstrated that the efficient inhibition of aggregation by rigid cationic substituents can be a very efficient tool for designing highly active PSs from the Pc family.

EXPERIMENTAL SECTION

General methods. The compounds 1,2,4-triazole, 2,6-bis(hydroxymethyl)-4-methylphenol, deuterated dimethylsulfoxide (DMSO-d_6), potassium carbonate (K_2CO_3), anhydrous zinc acetate, and unsubstituted ZnPc were purchased from

Sigma-Aldrich. In addition, 4,5-dichlorophthalonitrile and 5,6-dichloropyrazine-2,3-dicarbonitrile were obtained from TCI (Toshima, Japan). TLC was performed using Polygram SIL G/UV 254 TLC plates, and visualization was performed under ultraviolet light at 254 nm and 350 nm. Column chromatography was performed using Merck silica gel 60 of mesh size 0.040–0.063 mm. Anhydrous solvents were either supplied by Sigma-Aldrich and used as they were received or dried as described by Perrin.[40] ^{1}H and ^{13}C NMR spectra were recorded using a Bruker DPX 400 at 400 MHz and 100 MHz, respectively, and IR spectra were obtained with a Jasco 6300 FTIR. UV-Vis studies were performed on a Varian Cary 5 spectrometer and a Shimadzu UV-2600 spectrophotometer. Elemental analyses were performed using an Elementar Vario MICRO Cube. High-resolution mass analyses (HRMS) were performed on a Xevo G2-S QTof (Waters). In addition, clusters of peaks that corresponded to the calculated isotope composition of the molecular ion were observed by matrix-assisted laser desorption/ionization mass spectrometry (MALDI-TOF) *via* an ultrafleXtreme (Bruker). The MALDI-TOF mass data for Pcs and TPyzPzs are presented as the mass of the most intense peak in the cluster instead of the exact mass. Melting points were determined *via* differential scanning calorimetry (DSC) analyses on a Shimadzu DSC-50. Single-crystal data collections were performed on a Rigaku R-Axis Rapid diffractometer using filtered Mo-Kα radiation. The diffraction data were collected at a temperature of -123 °C (Oxford Cryosystems). All the studied compounds gave satisfactory elemental analyses with differences of less than 0.4% from the calculated values, indicating ≥95% purity.

General procedure for the synthesis of quaternized compounds. A solution of iodomethane (typically at least 6 eq. per triazole unit) and the corresponding non-quaternized compounds (**2, 3**, **7**, **8** or **11**-**13**) in dry DMF (10 mL per 0.6 g of material)

was heated at 80 °C under a nitrogen atmosphere for 24 h. The reaction mixture was poured into acetone (50 mL per 0.6 g of material) to give a precipitate that was collected by filtration. The crude product was refluxed in acetone and filtered three times. The precipitate of the Pc or TPyzPz compound was washed extensively with hot acetone and reprecipitated from MeOH/*n*-hexane to give highly pure complexes.

General procedure for the preparation of magnesium complexes 6 and 11. A mixture of magnesium (7 eq.) and a small crystal of iodine in anhydrous butanol (7 mL per 1.5 mmol of precursor) was refluxed for 4 h to prepare magnesium butoxide. The corresponding precursor (**2** or **3**, 1 eq.) was added, and the reflux was continued for another 3 h. The mixture was cooled to rt and poured into methanol-water (1:5). The green precipitate was collected by filtration and washed with hot water. The crude product was purified *via* column chromatography on silica gel to afford the desired product. The product was then dissolved in a small amount of acetone and added dropwise to hot water. The fine precipitate was collected by filtration and dried.

General procedure for the synthesis of metal-free ligands 7 and 12. *p*-Toluenesulfonic acid monohydrate (10 eq.) dissolved in THF (2 mL) was added to magnesium complex **6** or **11** (1 eq.) dissolved in chloroform (4 mL per 0.1 mmol). The mixture was stirred overnight at rt. The solvents were evaporated under reduced pressure, and the product was dissolved in a small amount of MeOH and added dropwise to hot water. The fine precipitate was collected by filtration, washed several times with hot acetone and dried.

General procedure for the synthesis of zinc complexes 8 and 13. A mixture of the corresponding metal-free ligand (**7** or **12**, 1 eq.) and anhydrous zinc(II) acetate (10 eq.) in dry pyridine (5 mL per 0.1 mmol of ligand) was refluxed for 3 h.

Subsequently, water was added to the reaction mixture. The fine precipitate was collected by filtration, washed with distilled water followed by hexane and dried.

2,6-Bis[(1*H*-1,2,4-triazol-1-yl)methyl]-4-methylphenol (1). A solution of 1,2,4-triazole (4.13 g, 0.06 mol) and 2,6-bis(hydroxymethyl)-4-methylphenol (5.04 g, 0.03 mol) in dioxane (10 mL) was refluxed for 24 h. Thereafter, the solvent was evaporated by removing the condenser, and the resulting material was recrystallized from acetone and then washed with hexane. White powder, yield 5.25 g (65%); mp 158.3 °C. Elemental analysis calcd (%) for $C_{13}H_{14}N_6O$: C, 57.77; H, 5.22; N, 31.09. Found: C, 57.57; H, 5.45; N, 30.70. FT-IR, ν_{max}/cm^{-1} 3104, 3013, 2723, 1775, 1762. ^1H NMR (400 MHz, DMSO-d_6, 25°C): δ= 2.14 (3H, s, CH_3), 5.37 (4H, s, CH_2), 6.82 (2H, s, Tri-H), 7.79 (2H, s, Tri-H), 8.54 (2H, s, Ar-H), 9.24 (1H, s, OH). ^{13}C NMR (100 MHz, DMSO-d_6, 25°C): δ=151.5, 150.3, 144.3, 130.2, 128.7, 124.1, 47.9, 20.1. *m/z* (EI) = 270.1 $[M]^+$ (100%). HRMS (ESI) calc. for $C_{13}H_{14}N_6O$ $[M]^+$: 270.1229, found 270.1224 $[M]^+$, 100%.

4,5-Bis{2,6-bis[(1*H*-1,2,4-triazol-1-yl)methyl]-4-methylphenoxy}phthalonitrile (2). Anhydrous cesium fluoride (5.70 g, 37.5 mmol) was added to a stirred solution of **1** (5.06 g, 18.75 mmol) and 4,5-dichlorophthalonitrile (1.43 g, 7.3 mmol) in dry DMF (20 mL). The reaction mixture was heated at 80 °C under nitrogen for 24 h. Upon cooling, the reaction mixture was poured into ice water (500 mL). The resulting precipitate was collected by filtration, recrystallized from THF and reprecipitated from DCM/hexane. Yellow Powder, yield 2.9 g (60%); mp. 236.6 °C. Elemental analysis calcd (%) for $C_{34}H_{28}N_{14}O_2 + 2H_2O$: C, 58.28; H, 4.60, N, 27.99. Found: C, 58.23; H, 4.40; N, 28.04. FT-IR, ν_{max}/cm^{-1} 3446, 3118, 3093, 2231 (CN), 1503. ^1H NMR (400 MHz, DMSO-d_6, 25°C): δ= 2.51 (6H, s, CH_3), 5.42 (8H, s, CH_2), 6.77 (2H, s, Pc-Ar-H), 7.17 (4H, s, Tri-H), 7.83 (4H, s, Tri-H), 8.55 (4H, s, Ar-H). ^{13}C

NMR (100 MHz, DMSO-d_6, 25°C): δ=151.4, 149.5, 145.6, 144.5, 137.0, 131.6, 129.4, 118.1, 115.3, 109.2, 47.2, 20.6. *m/z* (EI) = 664 $[M]^+$ (100%). HRMS (ESI) calc. for $C_{34}H_{28}N_{14}O_2$: 664.2520, found 664.2515 $[M]^+$, 100%.

5,6-Bis{2,6-bis[(1*H*-1,2,4-triazol-1-yl)methyl]-4-methylphenoxy}pyrazine-2,3-dicarbonitrile (3). Compound **1** (0.6 g, 2.22 mmol) was stirred in a mixture of dry acetone (50 mL) and dry pyridine (8 mL) at rt, and then a solution of 5,6-dichloropyrazine-2,3-dicarbonitrile (0.198 g, 1.00 mmol) in dry acetone (10 mL) was added. Stirring continued at rt overnight. The organic solvents were removed under reduced pressure. The resulting material was washed with water and filtered. The crude product was purified *via* column chromatography on silica gel and eluted with DCM:MeOH (10:2). The product was recrystallized from acetone/water. Silver crystals, yield 0.6 g (90 %); mp 148.1 °C. Elemental analysis calcd (%) for $C_{32}H_{26}N_{16}O_2 + H_2O$: C, 56.14; H, 4.12; N, 32.73. Found: C, 56.43; H, 3.85; N, 32.77. FT-IR, ν_{max}/cm^{-1}3424, 2241 (CN), 1610, 1439. ^{1}H NMR (400 MHz; DMSO-d_6, 25°C): δ/ ppm= 2.33 (6H, s, Me), 5.48 (8H, s, CH_2), 7.19 (4H, s, Ar-H), 7.88 (4H, s, Tri-H), 8.60 (4H, s, Tri-H). ^{13}C NMR (400 MHz; DMSO-d_6, 25°C): δ/ppm=151.4, 150.7, 144.6, 144.4, 137.6, 131.1, 129.1, 123.5, 113.1, 47.2, 20.5. *m/z* (EI) = 666.2 (M^+, 10%). HRMS (ESI) calc. for $C_{32}H_{26}N_{16}O_2$: 666.2425, found 666.2419 $[M]^+$, 100%.

4,5-Bis{4-methyl-2,6-bis[(4-methyl-1*H*-1,2,4-triazol-4-ium-1-yl)methyl]phenoxy}phthalonitrile tetraiodide (4). Compound **4** was prepared from the corresponding precursor **2** (0.66 g, 1 mmol) following the general procedure for quaternization. Yellow solid, yield 0.8 g (64%); mp 157.5 °C. Elemental analysis calcd (%) for $C_{38}H_{40}I_4N_{14}O_2 + 2H_2O$: C, 35.98; H, 3.50; N, 15.46. Found: C, 36.01; H, 3.61, N, 15.27. FT-IR, ν_{max}/cm^{-1} 3061, 2971, 2229 (CN), 1564, 1477; ^{1}H NMR

(400 MHz, DMSO-d_6, 25°C): δ= 2.38 (6H, s, CH_3), 3.91 (12H, s, N-CH_3), 5.60 (8H, s, CH_2), 7.19 (2H, s, Pc-Ar-H), 7.47 (4H, s, Tri-H)), 9.07 (4H, s, Tri-H)), 10.16 (4H, s, Ar-H). ^{1}H NMR (400 MHz, D_2O, 25°C): δ= 2.32 (24H, s, CH_3), 3.87 (48H, s, N-CH_3), 5.54 (32H, s, CH_2), 7.09 (8H, s, Pc-Ar-H), 7.43 (16H, s, Tri-H)), 8.68, (16H, s, Ar-H). ^{13}C NMR (100 MHz, DMSO-d_6, 25°C): δ=149.7, 145.9, 145.7, 143.9, 137.7, 132.7, 126.9, 119.3, 115.3, 110.1, 49.5, 34.5, 20.5. *m/z* (FAB) = 1233.4 $[M]^+$,1105.6 $[M\text{-}I^-]^+$.

5,6-Bis{4-methyl-2,6-bis[(4-methyl-1*H*-1,2,4-triazol-4-ium-1-yl)methyl]phenoxy}pyrazine-2,3-dicarbonitrile tetraiodide (5). Compound **5** was prepared from the corresponding precursor **3** (0.67 g, 1 mmol) following the general procedure for quaternization. Yellow solid, yield 0.59 g (53%); mp 334.9°C. Elemental analysis calcd (%) for $C_{36}H_{38}I_4N_{16}O_2$ + $3H_2O$: C, 33.56; H, 3.44; N, 17.39. Found: C, 33.25; H, 3.08, N, 17.15. FT-IR, ν_{max}/cm^{-1} 3429, 3116, 2237 (CN), 1581, 1435. ^{1}H NMR (400 MHz, DMSO-d_6, 25°C): δ/ ppm= 2.37 (6H, s, Me), 3.92 (12H, s, NMe), 5.68 (8H, s, CH_2), 7.40 (4H, s, Ar-H), 9.10 (4H, s, Tri-H)**)**, 10.17 (4H, s, Tri-H)). ^{1}H NMR (400 MHz, D_2O, 25°C), 2.31 (6H, s, Me), 3.88 (12H, s, NMe), 5.58 (8H, s, CH_2), 7.41 (4H, s, Ar-H), 8.72 (2H, s, Tri-H)). ^{13}C NMR (100 MHz; DMSO-d_6, 25°C): δ/ppm= 151.0, 146.0, 144.5, 143.8, 138.1, 131.9, 126.6, 124.2, 113.3, 49.6, 34.6, 20.4. *m/z* (FAB)=1107 $[M\text{-}I^-]^+$.

2,3,9,10,16,17,23,24-Octakis{2,6-bis[(1*H*-1,2,4-triazol-1-yl)methyl]-4-methylphenoxy}phthalocyaninato magnesium (II) (6). Compound **6** was prepared from precursor **2** (1.32 g, 2.00 mmol) following the general procedure for the magnesium complexes. The eluent system was DCM:MeOH:triethylamine (92:7:1). Green solid, yield 1.2 g (90%); mp > 300 °C. Elemental analysis calcd (%) for $C_{136}H_{112}N_{56}O_8Mg$ + $8H_2O$: C, 57.78; H, 4.56; N, 27.74. Found: 57.32; H, 4.47; N,

27.65. UV-vis (DMF): λ_{max}/nm (log ε): 289 (4.81), 363 (5.00), 613 (4.55), 679 (5.31). FT-IR, ν_{max}/cm^{-1}3425, 3115, 2923, 1478, 1451. ^{1}H NMR (400 MHz, DMSO-d$_6$, 25°C): δ= 2.51 (24H, s, CH_3), 5.66 (32H, s, CH_2), 7.25 (16H, s, Tri-H), 7.78 (16H, s, Tri-H), 7.99 (8H, s, Ar-H), 8.56 (16H, s, Pc-Ar-H). ^{13}C NMR (100 MHz, DMSO-d$_6$, 25°C): δ=152.4, 151.6, 150.1, 148.7, 147.5, 144.5, 136.2, 133.0, 131.0, 129.8, 47.5, 21.0. MS (MALDI-TOF) *m/z* 2681.98 $[M+H]^+$.

2,3,9,10,16,17,23,24-Octakis{2,6-bis[(1*H*-1,2,4-triazol-1-yl)methyl]-4-methylphenoxy}phthalocyanine (7). Compound **7** was prepared from **6** (1.34 g, 0.50 mmol) following the general procedure for the metal-free ligands. Green solid, yield 1.00 g (88%); mp > 300 °C. Elemental analysis calcd (%) for $C_{136}H_{114}N_{56}O_8$ + 5H_2O: C, 59.38; H, 4.54; N, 28.51. Found: 59.37; H, 4.48; N, 28.48. UV-vis (DMF): λ_{max}/nm (log ε): 292 (4.78), 351 (4.87), 608 (4.47), 669 (5.13), 700 (4.95). FT-IR, ν_{max}/cm^{-1} 3427, 3110, 2917, 1503, 1441. ^{1}H NMR (400 MHz, DMSO-d$_6$, 25°C): δ= −0.87 (s, 2H, pyrrole NH), 2.51 (24H, s, CH_3), 5.67 (32H, s, CH_2), 7.28 (16H, s, Tri-H), 7.75 (16H, s, Tri-H), 7.99 (8H, s, Ar-H), 8.57 (16H, s, Pc-Ar-H). ^{13}C NMR (100 MHz, DMSO-d$_6$, 25°C): δ=151.6, 149.7, 147.2, 144.5, 136.4, 131.1, 129.8, 107.6. MS (MALDI-TOF) *m/z* 2659.35 $[M]^+$.

2,3,9,10,16,17,23,24-Octakis{2,6-bis[(1*H*-1,2,4-triazol-1-yl)methyl]-4-methylphenoxy}phthalocyaninato zinc(II) (8). Compound **8** was prepared from ligand **7** (0.79 g, 0.30 mmol) following the general procedure for the zinc complexes. Bright-green, yield 0.74 g (90%); mp > 300 °C. Elemental analysis calcd (%) for $C_{136}H_{112}N_{56}O_8Zn$ + 6H_2O: C, 57.67; H, 4.41; N, 27.70. Found: 57.64; H, 4.30; N, 27.70. UV-vis (DMF): λ_{max}/nm (log ε): 289 (5.06), 362 (5.09), 612 (4.73), 678 (5.41). FT-IR, ν_{max}/cm^{-1} 3427, 3110, 2927, 1482, 1441. ^{1}H NMR (400 MHz, DMSO-d$_6$, 25°C): δ= 2.51 (24H, s, CH_3), 5.67 (32H, s, CH_2), 7.26 (16H, s, Tri-H), 7.77 (16H, s,

Tri-H), 7.98 (8H, s, Ar-H), 8.56 (16H, s, Pc-Ar-H). ^{13}C NMR (100 MHz, DMSO-d_6, 25°C): δ=152.1, 151.6, 148.8, 147.5, 144.5, 136.2, 132.7, 131.0, 129.8, 107.4, 47.5, 21.0. MS (MALDI-TOF) *m/z* 2721.99 $[M+H]^+$.

2,3,9,10,16,17,23,24-Octakis{4-methyl-2,6-bis[(4-methyl-1*H*-1,2,4-triazol-4-ium-1-yl)methyl]phenoxy}phthalocyanine hexadecaiodide (9). Compound **9** was prepared from the corresponding non-quaternized ligand **7** (0.54 g, 0.2 mmol) following the general procedure for quaternization. Green-blue solid, yield 0.45 g (45%); mp > 300 °C. Elemental analysis calcd (%) for $C_{152}H_{162}I_{16}N_{56}O_8$ + $8H_2O$: C, 35.97; H, 3.53; N, 15.45. Found: C, 36.11; H, 3.71; N, 15.07. UV-vis (DMF): λ_{max}/nm (log ε): 276 (4.89), 348 (4.96), 611 (4.59), 677 (5.33). UV-vis (H_2O): λ_{max}/nm (log ε) 291 (4.71), 349 (4.92), 612 (4.52), 670 (5.08), 697 (5.03). FT-IR, ν_{max}/cm^{-1} 3420, 3030, 1580, 1441. ^{1}H NMR (400 MHz, DMSO-d_6, 25°C): δ= 2.60 (24H, s, CH_3), 3.81 (48H, s, N-CH_3), 5.93 (32H, s, CH_2), 7.62 (16H, s, Tri-H), 8.22 (8H, s, Pc-Ar-H), 9.13 (16H, s, Tri-H), 10.29 (16H, s, Ar-H). ^{1}H NMR (400 MHz, D_2O, 25°C): δ= 2.62 (24H, s, CH_3), 3.44 (48H, s, N-CH_3), 5.80 (32H, d, CH_2), 7.68 (16H, s, Tri-H), 8.46 (8H, s, Pc-Ar-H), 8.54 (16H, s, Ar-H). ^{13}C NMR (100 MHz, DMSO-d_6, 25°C): δ=149.8, 147.5, 145.9, 143.9, 137.3, 132.0, 131.5, 127.2, 126.9, 50.2, 34.7, 21.0.

2,3,9,10,16,17,23,24-Octakis{4-methyl-2,6-bis[(4-methyl-1*H*-1,2,4-triazol-4-ium-1-yl)methyl]phenoxy}phthalocyaninato zinc(II) hexadecaiodide (10). Compound **10** was prepared from the corresponding non-quaternized complex **8** (0.55 g, 0.2 mmol) following the general procedure for quaternization. Blue solid, yield 0.5 g (50%); mp > 300 °C. Elemental analysis calcd (%) for $C_{152}H_{160}I_{16}N_{56}O_8Zn$ + $8H_2O$: C, 35.52; H, 3.45; N, 15.26. Found: C, 35.17; H, 3.58; N, 14.91. UV-vis (DMF) λ_{max}(nm), (log ε): 283 (4.88), 369 (5.12), 613 (4.71), 680 (5.49). UV-vis (H_2O) λ_{max}(nm), 288 (4.90), 359 (5.17), 614 (4.75), 681 (5.49). FT-IR, ν_{max}/cm^{-1} 3426, 3033,

1580, 1479, 1450. ^{1}H NMR (400 MHz, DMSO-d_6, 25°C): δ= 2.60 (24H, s, CH_3), 3.81 (48H, s, N-CH_3), 5.92 (32H, s, CH_2), 7.60 (16H, s, Tri-H), 8.24 (8H, s, Pc-Ar-H), 9.12 (16H, s, Tri-H), 10.27 (16H, s, Ar-H). ^{1}H NMR (400 MHz, D_2O, 25°C): δ= 2.64 (24H, s, CH_3), 3.39 (48H, s, N-CH_3), 5.80 (32H, d, CH_2), 7.70 (16H, s, Tri-H), 8.45 (8H, s, Pc-Ar-H), 8.51 (16H, s, Ar-H). ^{13}C NMR (100 MHz, DMSO-d_6, 25°C): δ=152.3, 148.8, 148.0, 145.9, 143.9, 137.1, 133.3, 131.9, 127.3, 50.0, 34.7, 21.0.

2,3,9,10,16,17,23,24-Octakis{2,6-bis[(1*H*-1,2,4-triazol-1-yl)methyl]-4-methylphenoxy}tetrapyrazinoporphyrazinato magnesium (II) (**11**). Compound **11** was prepared from precursor **3** (0.80 g, 1.20 mmol) following the general procedure for the magnesium complexes. The eluent system was DCM:MeOH:triethylamine (80:20:5). Yield 0.4 g (50 %); mp > 300 °C. Elemental analysis calcd (%) for $C_{128}H_{104}N_{64}O_8Mg + 10H_2O$: C, 53.55; H, 4.35; N, 31.22. Found: C, 53.54; H, 4.24; N, 30.80. UV-vis (DMF): λ_{max}/nm (log ε): 365 (4.95), 573 (4.34), 630 (5.16). FT-IR, ν_{max}/cm^{-1}3435.56, 3119.3, 1634.38. ^{1}H NMR (400 MHz; DMSO-d_6, 25°C) δ/ ppm= 2.54 (24H, s, Me), 5.77 (32H, s, CH_2), 7.34 (16H, s, Ar-H), 7.67(16H, s, Tri-H), 8.79 (16H, s, Tri-H). ^{13}C NMR (400 MHz; DMSO-d_6, 25°C): δ/ ppm= 151.2, 150.8, 148.8, 146.2, 144.4, 142.5, 136.5, 130.8, 130.2, 48.0, 21.0. MS (MALDI-TOF) *m/z* 2712.8 $[M+Na]^+$, 5402.5 $[2M+Na]^+$.

2,3,9,10,16,17,23,24-Octakis{2,6-bis[(1*H*-1,2,4-triazol-1-yl)methyl]-4-methylphenoxy}tetrapyrazinoporphyrazine (12). Compound **12** was prepared from **11** (0.10 g, 0.04 mmol) following the general procedure for the metal-free ligands. Green solid, yield 0.09 g (91 %); mp > 300 °C. Elemental analysis calcd (%) for $C_{128}H_{106}N_{64}O_8 + 10H_2O$: C, 53.97; H, 4.46; N, 31.47. Found: C, 54.11; H, 4.44; N, 31.19. UV-vis (DMF): λ_{max}/nm (log ε): 365 (5.01), 576 (4.38), 632 (5.15). FT-IR, ν_{max}/cm^{-1} 3433.64, 3117.37, 1632. ^{1}H NMR (400 MHz; DMSO-d_6, 25°C) δ/ ppm= -

1.87 (2H, s), 2.54 (24H, s, Me), 5.76 (32H, s, CH_2), 7.35 (16H, s, Ar-H), 7.664, 7.675 (16H, d, Tri-H), 8.723, 8.756 (16H, d, Tri-H). ^{13}C NMR (400 MHz; DMSO-d_6, 25°C) δ/ ppm= 151.2, 151.0, 149.5, 146.3, 144.5, 142.7, 136.3, 130.6, 130.2, 48.1, 21.1. MS (MALDI-TOF) *m/z* 2667.58 $[M]^+$.

2,3,9,10,16,17,23,24-Octakis{2,6-bis[(1*H*-1,2,4-triazol-1-yl)methyl]-4-methylphenoxy}tetrapyrazinoporphyrazinato zinc(II) (13). Compound **13** was prepared from ligand **12** (0.10 g, 0.04 mmol) following the general procedure for the zinc complexes. Deep sky blue solid, yield 0.1 g (97 %); mp > 300 °C. Elemental analysis calcd (%) for $C_{128}H_{104}N_{64}O_8Zn$ + 11 H_2O: C, 52.47; H, 4.33; N, 30.59. Found: C, 52.78; H, 3.99; N, 30.13. UV-vis (DMF): λ_{max}/nm (log ε): 371 (4.94), 574 (4.31), 630 (5.51). FT-IR, ν_{max}/cm^{-1} 3438, 3125, 1634. ^{1}H NMR (400 MHz; DMSO-d_6, 25°C): δ/ ppm= 2.5 (24H, s, Me), 5.76 (32H, s, CH_2), 7.33 (16H, s, Ar-H), 7.69(16H, s, Tri-H), 8.74 (16H, s, Tri-H). ^{13}C NMR (400 MHz; DMSO-d_6, 25°C): δ/ ppm= 151.3, 149.4, 146.0, 144.5, 142.5, 136.4, 130.2, 47.9, 21.0. MS (MALDI- TOF) *m/z* 2752.7 $[M+Na]^+$, 5484.3 $[2M+Na]^+$. Compound **13** was prepared also by direct cyclotetramerization with zinc(II) acetate, but in a low yield, as discussed below.

Alternative method for preparation of 13. A mixture of **3** (1 g, 1.50 mmol) and anhydrous zinc(II) acetate (0.096 g, 0.52 mmol) in dry quinoline (5 mL) was heated at 170 °C under a nitrogen atmosphere for 5 h. The reaction mixture was cooled to rt and poured into diethyl ether (100 mL). The precipitate was collected by filtration and washed with hot water. The crude product was purified *via* column chromatography on silica gel and eluted with DCM:MeOH:pyridine (80:20:10). The product was collected by filtration, washed with hot distilled water and dried. Deep sky-blue solid, yield 0.1 g (10%).

2,3,9,10,16,17,23,24-Octakis{4-methyl-2,6-bis[(4-methyl-1*H*-1,2,4-triazol-4-ium-1-yl)methyl]phenoxy}tetrapyrazinoporphyrazinato magnesium(II) hexadecaiodide (14). Compound **14** was prepared from the corresponding non-quaternized complex **11** (0.54 g, 0.2 mmol) following the general procedure for quaternization. Cadet blue solid, yield 0.65 g (65%); mp > 300 °C. Elemental analysis calcd (%) for $C_{144}H_{152}I_{16}N_{64}O_8Mg + 4H_2O$: C, 34.36; H, 3.20; N, 17.81. Found C, 34.43; H, 3.57; N, 17.79. UV-vis (DMF) λ_{max}(nm), (log ε): 371 (5.00), 587 (4.40), 638 (4.94). UV-vis (H_2O) λ_{max}(nm), 376 (5.11), 577 (4.44), 634 (5.24). FT-IR, ν_{max}/cm^{-1} 3432, 3116, 1581, 1472, 1386. ^{1}H NMR (400 MHz, DMSO-d_6, 25°C) δ/ ppm= 2.66 (24H, s, Me), 3.52 (48H, s, NMe), 6.17 (32H, s, CH_2), 7.59 (16H, s, Ar-H), 9.08 (16H, s, Tri-H), 10.30 (16H, s, Tri-H). ^{1}H NMR (400 MHz, D_2O, 25°C) δ/ ppm= 2.61 (24H, s, Me), 3.44 (48H, s, NMe), 5.92 (32H, s, CH_2), 7.65 (16H, s, Ar-H), 8.52 (16H, s, Tri-H). ^{13}C NMR (100 MHz; DMSO-d_6, 25°C) δ/ ppm= 150.9, 148.6, 146.3, 145.6, 144.0, 143.3, 137.4, 132.3, 127.4, 51.0, 34.8, 21.2.

2,3,9,10,16,17,23,24-Octakis{4-methyl-2,6-bis[(4-methyl-1*H*-1,2,4-triazol-4-ium-1-yl)methyl]phenoxy}tetrapyrazinoporphyrazine hexadecaiodide (15). Compound **15** was prepared from the corresponding non-quaternized ligand **12** (0.53 g, 0.2 mmol) following the general procedure for quaternization. Dark green solid, yield 0.54 g (54 %); mp > 300 °C. Elemental analysis calcd (%) for $C_{144}H_{154}I_{16}N_{64}O_8$: C, 35.01; H, 3.14; N, 18.15. Found: C, 35.19; H, 3.54; N, 18.18. UV-vis (DMF) λ_{max}(nm), (log ε): 361 (4.89), 582 (4.31), 640 (4.88). UV-vis (H_2O) λ_{max}(nm), 357 (4.96), 584 (4.35), 643 4.99). FT-IR, ν_{max}/cm^{-1} 3432, 3113, 1580, 1470. ^{1}H NMR (400 MHz, DMSO-d_6, 25°C) δ/ ppm= -0.47 (2H, s), 2.65 (24H, s, Me), 3.51 (48H, s, NMe), 6.06 (32H, s, CH_2), 7.62 (16H, s, Ar-H), 8.96 (16H, s, Tri-H), 10.24 (16H, s, Tri-H). ^{1}H NMR (400 MHz, D_2O, 25°C) δ/ ppm= 2.54 (24H, s, Me), 3.95 (48H, s,

NMe), 5.88 (32H, s, CH_2), 7.63 (16H, s, Ar-H), 8.46 (16H, s, Tri-H). ^{13}C NMR (100 MHz; DMSO-d_6, 25°C) δ/ ppm= 150.4, 146.7, 145.6, 143.3, 142.9, 137.4, 132.6, 127.2, 50.6, 34.6, 21.1.

2,3,9,10,16,17,23,24-Octakis{4-methyl-2,6-bis[(4-methyl-1*H*-1,2,4-triazol-4-ium-1-yl)methyl]phenoxy}tetrapyrazinoporphyrazinato zinc(II) hexadecaiodide (16). Compound **16** was prepared from the corresponding non-quaternized complex **13** (0.55 g, 0.2 mmol) following the general procedure for quaternization. Green-blue solid, yield 0.55 g (55%); mp > 300 °C. Elemental analysis calcd (%) for $C_{144}H_{152}I_{16}N_{64}O_8Zn$ + $4H_2O$: C, 34.08; H, 3.18; N, 17.66. Found: C, 33.68; H, 3.26; N, 17.42. UV-vis (DMF) λ_{max}(nm), (log ε): 373 (5.12), 578 (4.45), 633 (5.18). UV-vis (H_2O) λ_{max}(nm), 365 (5.20), 577 (4.51), 633 (5.34). FT-IR, ν_{max}/cm^{-1} 3427, 3113, 1580, 1472, 1388. ^{1}H NMR (400 MHz, DMSO-d_6, 25°C) δ/ ppm= 2.66 (24H, s, Me), 3.64 (48H, s, NMe), 6.11 (32H, s, CH_2), 7.62 (16H, s, Ar-H), 9.05 (16H, s, Tri-H), 10.27 (16H, s, Tri-H). ^{1}H NMR (400 MHz, D_2O, 25°C) δ/ ppm= 2.6 (24H, s, Me), 3.43 (48H, s, NMe), 5.92 (32H, s, CH_2), 7.7 (16H, s, Ar-H), 8.52 (16H, s, Tri-H). ^{13}C NMR (100 MHz; DMSO-d_6, 25°C) δ/ ppm= 151.2, 149.2, 146.4, 145.7, 143.4, 143.1, 137.5, 132.4, 127.3, 50.8, 34.7, 21.1.

Fluorescence measurements. Steady-state and time-resolved fluorescence were measured using an FS5 spectrofluorimeter (Edinburgh Instruments) equipped with a TCSPC module and R928P photomultiplier. A Xe lamp was used for steady-state measurements, and the samples and reference compound were excited at 612 nm (**6-10**) or 595 nm (**11-16**). Unsubstituted ZnPc in THF was used as the reference compound for the determination of fluorescence quantum yields ($\Phi_{F(ZnPc)}$ = 0.32 in THF[21]) by the comparative method. The determination of Φ_F was performed in triplicate, and the data represent the mean of these measurements. The estimated

experimental error was ± 10%. Absorption of the samples at the excitation wavelength was kept below 0.05 and at a Q-band maximum below 0.1 to avoid the inner-filter effect. The results of Φ_F were corrected for the refractive indices of the solvents. For time-resolved measurements, the samples were excited at 371.2 nm using an EPL-375 picosecond pulsed diode laser (pulse width: 68 ps).

Singlet oxygen quantum yield. The singlet oxygen quantum yields (Φ_Δ) in DMF were determined by the comparative method based on the decomposition of a chemical probe for singlet oxygen (1,3-diphenylisobenzofuran) and using ZnPc as the reference compound ($\Phi_{\Delta(ZnPc)}$ = 0.56 in DMF[28]). Details of the method are described elsewhere.[41] All the determinations were performed in triplicate, and the data represent the mean of the measurements. The estimated experimental error was ± 10%.

Determination of log *P*. Stock solutions of all PSs were prepared in DMF at a concentration of 300 μM. A mixture of water (400 μL) and *n*-octanol (400 μL) was prepared in a plastic vial, and 20 μL of the DMF stock solution of PS was added. The mixture was vortexed for 5 min at rt and then centrifuged (10 000 rpm, 10 min, rt). The octanol and water phases were separated (the middle part between the layers was discarded), and 20 μL of each layer was diluted in DMF (2 mL). The emission spectra of these DMF solutions were measured (λ_{ex} = 370 nm), and the log *P* was calculated: log *P* = log (F_{OctOH}/F_{H2O}), where F_{OctOH} and F_{H2O} are the integrated emission spectra for the *n*-octanol and water layers, respectively. Compounds **7** and **11-13** precipitated in the interphase during the measurements, and log *P* could therefore not be determined.

Cell culture and sample preparation. The human cervical carcinoma (HeLa), human colorectal carcinoma (HCT 116) and human breast adenocarcinoma (MCF-7)

cell lines were purchased from the American Type Cell Culture Collection (ATCC; United States). The immortalized human keratinocytes (HaCaT) were obtained from Cell Lines Service (Eppelheim, Germany). The cells were cultured in Dulbecco's modified Eagle's medium (DMEM) without phenol red (Lonza, Belgium) and supplemented with 10% heat-inactivated FBS (Sigma), 1% penicillin/streptomycin solution (Lonza), 10 mM HEPES buffer (Sigma, Germany), and 4 mM L-glutamine (Lonza)—further referred to as the cell culture medium. The cell lines were cultured in 75 cm^2 tissue culture flasks (TPP, Switzerland) and maintained in a CO_2 incubator at 37 °C in a humidified atmosphere of 5% CO_2 and subcultured every 3−4 days. For the cytotoxicity experiments (phototoxicity and dark toxicity), cells were seeded into 96-well plates (TPP) at a density of 7.5×10^3 (HeLa and MCF-7) or 1.0×10^4 (HaCaT and HCT 116) cells per well for 24 h.

Stock solutions of the investigated compounds were prepared in the cell culture medium at a concentration of 1.0 mM (**9**, **10** and **14**-**16**) or in DMSO at a concentration of 10 mM (**6**-**8**, **11**-**13**) and were sterilized by filtration through 0.22 μm syringe filters. No measurable change in concentration was detected after passage through the filter based on the absorption spectra measured before and after filtration.

Cytotoxicity experiments. Dark toxicities (inherent toxicities of the studied PSs in the absence of any light) were assayed over a wide concentration range after 24 h incubation with HeLa cells. Cell viability was determined using the Neutral Red (NR, Sigma) uptake assay based on the ability of the living cells to incorporate NR into their intact lysosomes. The soluble NR was measured as its optical density at λ = 540 nm using a Tecan Infinite 200 M plate reader (Tecan, Austria). The viability of each experimental group was expressed as the percentage of the untreated controls incubated under the same conditions (100%). After NR staining of the cells (before

lysis), the cells were briefly investigated under an inverted microscope to verify qualitative changes in cellular morphology and NR uptake into intact lysosomes. These observations were in accordance with subsequent quantitative measurements. False positivity in absorbance measurements using the NR uptake assay method was also eliminated. After incubation with the PS, the cells were killed with a lethal concentration of H_2O_2 (200 μM) and stained with the NR uptake assay protocol used in all the cellular viability experiments. No absorbance interference of any PS with NR over the entire concentration scale (PDT and dark toxicity experiments) was observed.

For the photodynamic treatment experiments (phototoxicity), HeLa, MCF-7, HCT 116 and HaCaT cells were incubated with various concentrations of the studied compounds for 12 h. The cells were then washed with prewarmed serum-free cell culture medium, fresh cell culture medium was added, and the cells were irradiated for 15 min using a 450 W ozone-free Xe lamp (Newport) with its intensity reduced to 400 W that was equipped with a long-pass filter (Newport OG570) and an 8-cm water filter to cut off undesirable wavelengths and heat radiation ($\lambda > 570$ nm, 12.4 mW cm^{-2}, 15 min, 11.2 J cm^{-2}). Cellular viability was measured after an additional 24 h by NR as previously described. At least five independent experiments, each in quadruplicate, were performed.

The concentrations of the tested compounds that induced a 50% viability decrease after treatment under the dark conditions (TC_{50}, the median toxic concentration) or after the photodynamic treatment (EC_{50}, the median effective concentration) were calculated using GraphPad Prism software (version 6.07; GraphPad Software, Inc., San Diego, CA, USA) for each independent experiment. The data in Table 2 are presented as the means ± standard deviation of these values.

In another photodynamic experiment in HeLa cells, EC_{50} values were also determined with different irradiation times of 5 min and 30 min, which resulted in total fluences of 3.7 J cm^{-2} and 22.4 J cm^{-2}.

Uptake by the cells. HeLa cells were seeded into 6 cm Petri dishes (TPP) at a density of 5.0×10^5 cells per dish. The cells were left to grow for 24 h, the medium was removed, and 5 mL of a 4 μM solution of **10** or **16** or a 1 μM solution of **8** in cell culture medium were added (**8** was prepared from a 10 mM stock solution in DMSO). The cells were washed two times with 5 mL of prewarmed phosphate-buffered saline (PBS; Sigma) after 0, 0.002, 0.5, 1, 2, 4, 6, 8 and 12 h. Fresh serum-free cell culture medium (5 mL) was added, and the cells were scraped and transferred to 15 mL centrifugation tubes (TPP) and centrifuged for 5 min at 70 g. The supernatant was replaced with 2 mL of fresh serum-free cell culture medium, and the pellet was gently resuspended and centrifuged again. This process was repeated two times. After the last centrifugation, the medium was replaced with 500 μL of MQ-water (Millipore, USA) (for **10** and **16**) or with 500 μL of DMSO (for **8**). Lysis of the cells in water was performed overnight at -80 °C. The samples were quickly thawed at 37 °C and frozen at -80 °C for an additional 2 h. The fluorescence of the samples (λ_{ex} = 370 nm, λ_{em} = 686, 690 and 639 nm for **8**, **10** and **16**, respectively) was measured using an FS5 spectrofluorimeter and was plotted against the incubation time. Nonspecific fluorescence was excluded by the control experiments. Emission from endogenous chromophores in the cells at 659 nm did not interfere with the measurement. A calibration curve was constructed using dilutions of the dye stock solution into the cell lysate prepared as described above (*i.e.,* in water or in DMSO). The uptake experiments were performed in duplicate. Experiments were performed in dark the entire time.

The amounts of protein in the samples were assessed using the BCA (bicinchoninic acid) method. A calibration curve was created using bovine serum albumin dissolved in MQ-water at concentrations of 0, 50, 100, 200, 400, 600, 800 and 1000 μg/mL. A working solution of BCA (4% $CuSO_4 \cdot 6H_2O$ mixed *ad hoc* with bovine serum albumin stock solution at a 1:50 ratio) was added to 10 μL of the samples. Absorbance (562 nm) was measured after 30 min incubation at 37 °C using a Tecan Infinite M 200 plate reader.

Subcellular localization experiments. HeLa cells were seeded onto Petri dishes suitable for confocal microscopy (WillCo Wells, Netherlands) in cell culture medium at a density of 7.5×10^4 cells per dish and were incubated for 12 h with a 4 μM solution of **9, 10** or **14-16** or a 1 μM solution of **6-8** or **11-13** in an incubator (37 °C, 5% CO_2 atmosphere, constant humidity). The medium was removed, cells were washed twice with prewarmed PBS, and fresh medium was added. LysoTracker Blue DND-22 (Molecular Probes, 0.25 μM) and MitoTracker Green FM (Molecular Probes, 0.2 μM) were added, and the cells were incubated for an additional 15 min. After incubation, the cells were rinsed twice with prewarmed PBS, fresh SFM was added, and the samples were immediately placed in a stage-top CO_2 incubator (Okolab, Italy) and examined. The subcellular localization of **10** was further confirmed using LSCM: A) Cells were transfected with Rab7a-GFP (CellLight® Late Endosomes-GFP, BacMam 2.0, Molecular Probes, 50 particles per cell) and Lamp1-RFP (CellLight® Lysosomes-RFP, BacMam 2.0, Molecular Probes, 50 particles per cell) for 16 h prior to the addition of **10**; B) Cells were transfected with *N*-acetylgalactosaminyltransferase-2-RFP (GALNT2-RFP, CellLight® Golgi-RFP, BacMam 2.0, Molecular Probes, 50 particles per cell) for 16 h prior to the addition of the PS, incubated with **10** for 12 h and, after washing, incubated additionally with

BODIPY FL Glibenclamide (ER-Tracker Green, Molecular Probes, 1 μM) for 15 min. A Nikon A1+ (Nikon, Japan) confocal system equipped with NIS Elements AR 4.20 software (Laboratory Imaging, Czech Republic) was employed to visualize all structures in live cells using 405 nm, 488 nm and 561 nm lasers; the PSs were visualized using a 640 nm laser. A single confocal plane of focus (pinhole diameter = 26.8 μm) was taken, and NIS Elements AR 4.20 software was used to create a fluorescence intensity profile.

Morphological changes – live-cell imaging. For morphology changes evaluated by live-cell LSCM imaging, HeLa cells were seeded onto Petri dishes suitable for confocal microscopy (WillCo Wells, Netherlands) in cell culture medium at a density of 7.5×10^4 HeLa cells and were left to grow for 24 h prior to the addition of **10**. Incubation with PS (at a concentration of $EC_{15} = 4.5$ nM or $EC_{85} = 25.1$ nM) was performed for 12 h, and irradiation was performed as described for the phototoxicity studies. After 1 h or 24 h, the cells were washed with prewarmed serum-free cell culture medium; stained for 15 min with 0.3 μM MitoTracker Red CMXRos (Molecular Probes), 1 μM ER-Tracker Green and 4 nM Hoechst 33342; and washed twice with prewarmed serum-free cell culture medium. Next, fresh medium was added. A sample was placed in a stage-top incubator, and photomicrographs were obtained using the Nikon A1+ confocal system with 405, 488, and 561 nm lasers. DIC images were acquired using a transmission detector. Four confocal planes were typically taken to cover the entire volume of the cells in the field of view. The pinhole diameter was set at 30.7 μm, and the laser power was kept as low as possible to prevent undesirable photodamage.

Morphological changes – fixed specimen. HeLa cells were seeded onto cover glass chamber slides (Eppendorf, Germany) at a density of 2.0×10^4 cells per well.

Incubation with **10** and irradiation were performed as described above. Fixation of the specimens was performed after 1 h and 24 h using prewarmed 4% paraformaldehyde dissolved in cell culture medium for 15 min at 37 °C. Cells were rinsed three times for 5 min with Dulbecco's phosphate-buffered saline (dPBS, pH = 7.4) and were permeabilized using 0.5% Triton X-100 for 15 min at rt. Cells were washed three times for 5 min with dPBS and blocked for 60 min at rt with 3% bovine serum albumin in dPBS. Incubation with 2 μg/mL α-tubulin antibody, Alexa Fluor 488 conjugate (Thermo Fisher Scientific) and 5 U/mL Alexa Fluor 555 phalloidin (Molecular Probes) in 3% bovine serum albumin was performed for 90 min. Specimens were rinsed and stained with 4 nM Hoechst 33342 in dPBS for 15 min and subsequently rinsed again and washed for 5 min with MQ-water to remove excess salts. Mounting was performed after drying using ProLong Gold antifade mountant (Molecular Probes) overnight at rt. Photomicrographs were obtained using the Nikon A1+ confocal system. Eight confocal planes were typically taken to cover the entire volume of the specimens using 405, 488, and 561 nm lasers. The pinhole diameter was set at 30.7 μm.

Flow cytometry assessment of cell death. HeLa cells were seeded onto 60 mm Petri dishes (TPP) and incubated for 12 h with **10** at concentrations corresponding to its EC_{15} and EC_{85} values. Irradiation was performed under the same conditions used in the phototoxicity experiments. The cells were then harvested by trypsinization, followed by scraping and co-stained with PI (3 μM, Molecular Probes) and annexin V−Alexa Fluor 488 (1 vol%, Molecular Probes) for 15 min at 37 °C. Cells that were negative or positive for red and/or green fluorescence were counted using an Accuri C6 flow cytometer (Accuri Cytometers Europe Ltd., United Kingdom) at 20 min and

1, 3, 6 and 24 h after irradiation. Ten thousand events were collected per analysis. The experiment was performed in triplicate.

Interaction with serum proteins. The interactions of **8-10** and **16** with serum proteins were studied by means of absorption and fluorescence spectroscopy. The compounds were dissolved in serum-free cell culture medium (in case of **8**, using a 300 μM DMF stock solution) at a concentration of approximately 1 μM. Absorption and emission spectra (λ_{ex} = 370 nm) were subsequently measured after each small addition of FBS up to approximately 12% of FBS in the medium. The typical amount of FBS in cell culture media is 10%.

Data analysis. The statistical analysis was performed with the GraphPad Prism statistical program (version 6.07; GraphPad Software, Inc. San Diego, CA). One-way ANOVA with Bonferroni's multiple comparison post hoc test was used. The results were compared with the control samples, and the mean values were considered significant if (*) $p < 0.05$, (**) $p < 0.01$, and (***) $p < 0.001$.

ASSOCIATED CONTENT

Supporting Information. NMR spectra, additional graphs and photos from the photophysical and biological evaluations, and details on the X-ray structures. This material is available free of charge *via* the Internet at http://pubs.acs.org.

AUTHOR INFORMATION

Corresponding Author

* saad.makhseed@ku.edu.kw; tel: +965 24985538, * petr.zimcik@faf.cuni.cz, tel: +420 495067257.

ACKNOWLEDGMENT

The P.I. (Dr. Saad Makhseed) and the other researchers are grateful for the financial support from the Kuwait Foundation for the Advancement of Science (Grant Number P114-14-SC01) and the RSP unit general facilities of the Faculty of Science GFS (GS 01/01, GS 02/01, GS 03/01, GS 01/03, GS 01/05, GS 02/13). Chemistry department at Kuwait University is highly acknowledged for using MALDI-TOF. Nanoscopy Science Center is highly acknowledged for using TEM.

ABBREVIATIONS

BCA, bicinchoninic acid; DIC, differential interference contrast; dPBS, Dulbecco's phosphate-buffered saline; FBS, fetal bovine serum; LSCM, laser scanning confocal microscopy; NR, neutral red; Pc, phthalocyanine; PDT, photodynamic therapy; PI, propidium iodide; PpIX, protoporphyrin IX; PS, photosensitizer; TC_{50}, half maximal toxic concentration; TPyzPz, tetrapyrazinoporphyrazine; ZnPc, unsubstituted zinc phthalocyanine.

REFERENCES

(1) Agostinis, P.; Berg, K.; Cengel, K. A.; Foster, T. H.; Girotti, A. W.; Gollnick, S. O.; Hahn, S. M.; Hamblin, M. R.; Juzeniene, A.; Kessel, D.; Korbelik, M.; Moan, J.; Mroz, P.; Nowis, D.; Piette, J.; Wilson, B. C.; Golab, J. Photodynamic therapy of cancer: An update. *Ca-Cancer J. Clin.* **2011**, *61*, 250-281.

(2) Abrahamse, H.; Hamblin, M. R. New photosensitizers for photodynamic therapy. *Biochem. J.* **2016**, *473*, 347-364.

(3) Dabrowski, J. M.; Arnaut, L. G. Photodynamic therapy (PDT) of cancer: from local to systemic treatment. *Photochem. Photobiol. Sci.* **2015**, *14*, 1765-1780.

(4) Lobo, A. C. S.; Silva, A. D.; Tomé, V. A.; Pinto, S. M. A.; Silva, E. F. F.; Calvete, M. J. F.; Gomes, C. M. F.; Pereira, M. M.; Arnaut, L. G. Phthalocyanine

labels for near-infrared fluorescence imaging of solid tumors. *J. Med. Chem.* **2016**, *59*, 4688-4696.

(5) Sekkat, N.; van den Bergh, H.; Nyokong, T.; Lange, N. Like a bolt from the blue: Phthalocyanines in biomedical optics. *Molecules* **2012**, *17*, 98-144.

(6) Lukyanets, E. A. Phthalocyanines as photosensitizers in the photodynamic therapy of cancer. *J. Porphyrins Phthalocyanines* **1999**, *3*, 424-432.

(7) Lau, J. T. F.; Lo, P.-C.; Jiang, X.-J.; Wang, Q.; Ng, D. K. P. A Dual activatable photosensitizer toward targeted photodynamic therapy. *J. Med. Chem.* **2014**, *57*, 4088-4097.

(8) Chow, S. Y. S.; Lo, P.-C.; Ng, D. K. P. An acid-cleavable phthalocyanine tetramer as an activatable photosensitiser for photodynamic therapy. *Dalton Trans.* **2016**, *45*, 13021-13024.

(9) Zhen, Z.; Tang, W.; Guo, C.; Chen, H.; Lin, X.; Liu, G.; Fei, B.; Chen, X.; Xu, B.; Xie, J. Ferritin nanocages to encapsulate and deliver photosensitizers for efficient photodynamic therapy against cancer. *ACS Nano* **2013**, *7*, 6988-6996.

(10) Skupin-Mrugalska, P.; Piskorz, J.; Goslinski, T.; Mielcarek, J.; Konopka, K.; Düzgüneş, N. Current status of liposomal porphyrinoid photosensitizers. *Drug Discovery Today* **2013**, *18*, 776-784.

(11) Lucky, S. S.; Soo, K. C.; Zhang, Y. Nanoparticles in photodynamic therapy. *Chem. Rev.* **2015**, *115*, 1990-2042.

(12) Lau, J. T. F.; Lo, P.-C.; Fong, W.-P.; Ng, D. K. P. Preparation and photodynamic activities of silicon(IV) phthalocyanines substituted with permethylated β-cyclodextrins. *Chem.–Eur. J.* **2011**, *17*, 7569-7577.

(13) Jiang, X. J.; Yeung, S. L.; Lo, P. C.; Fong, W. P.; Ng, D. K. P. Phthalocyanine -polyamine conjugates as highly efficient photosensitizers for photodynamic therapy. *J. Med. Chem.* **2011**, *54*, 320-330.

(14) Venkatramaiah, N.; Pereira, P. M. R.; Almeida Paz, F. A.; Ribeiro, C. A. F.; Fernandes, R.; Tome, J. P. C. Dual functionality of phosphonic-acid-appended phthalocyanines: inhibitors of urokinase plasminogen activator and anticancer photodynamic agents. *Chem. Commun.* **2015**, *51*, 15550-15553.

(15) Kucinska, M.; Skupin-Mrugalska, P.; Szczolko, W.; Sobotta, L.; Sciepura, M.; Tykarska, E.; Wierzchowski, M.; Teubert, A.; Fedoruk-Wyszomirska, A.; Wyszko, E.; Gdaniec, M.; Kaczmarek, M.; Goslinski, T.; Mielcarek, J.; Murias, M. Phthalocyanine derivatives possessing 2-(morpholin-4-yl)ethoxy groups as potential agents for photodynamic therapy. *J. Med. Chem.* **2015**, *58*, 2240-2255.

(16) Dumoulin, F.; Durmus, M.; Ahsen, V.; Nyokong, T. Synthetic pathways to water-soluble phthalocyanines and close analogs. *Coord. Chem. Rev.* **2010**, *254*, 2792-2847.

(17) Ongarora, B. G.; Zhou, Z.; Okoth, E. A.; Kolesnichenko, I.; Smith, K. M.; Vicente, M. G. H. Synthesis, spectroscopic, and cellular properties of alpha-pegylated cis-A(2)B(2)- and A(3)B-types ZnPcs. *J. Porphyrins Phthalocyanines* **2014**, *18*, 1021-1033.

(18) Makhseed, S.; Machacek, M.; Alfadly, W.; Tuhl, A.; Vinodh, M.; Simunek, T.; Novakova, V.; Kubat, P.; Rudolf, E.; Zimcik, P. Water-soluble non-aggregating zinc phthalocyanine and in vitro studies for photodynamic therapy. *Chem. Commun.* **2013**, *49*, 11149-11151.

(19) Machacek, M.; Demuth, J.; Cermak, P.; Vavreckova, M.; Hruba, L.; Jedlickova, A.; Kubat, P.; Simunek, T.; Novakova, V.; Zimcik, P. Tetra(3,4-

pyrido)porphyrazines caught in the cationic cage: Toward nanomolar active photosensitizers. *J. Med. Chem.* **2016**, *59*, 9443-9456.

(20) Linstead, R. P.; Noble, E. G.; Wright, J. M. Phthalocyanines. IX. Derivatives of thiophene, thionaphthene, pyridine and pyrazine, and a note on the nomenclature. *J. Chem. Soc.* **1937**, 911-921.

(21) Zimcik, P.; Novakova, V.; Kopecky, K.; Miletin, M.; Uslu Kobak, R. Z.; Svandrlikova, E.; Váchová, L.; Lang, K. Magnesium azaphthalocyanines: An emerging family of excellent red-emitting fluorophores. *Inorg. Chem.* **2012**, *51*, 4215-4223.

(22) Vashurin, A.; Filippova, A.; Znoyko, S.; Voronina, A.; Lefedova, O.; Kuzmin, I.; Maizlish, V.; Koifman, O. A new water-soluble sulfonated cobalt(II) phthalocyanines: Synthesis, spectral, coordination and catalytic properties. *J. Porphyrins Phthalocyanines* **2015**, *19*, 983-996.

(23) Makhseed, S.; Ibrahim, F.; Samuel, J.; Helliwell, M.; Warren, J. E.; Bezzu, C. G.; McKeown, N. B. Clathrate formation from octaazaphthalocyanines possessing bulky phenoxyl substituents: A new cubic crystal containing solvent-filled, nanoscale voids. *Chem.-Eur. J.* **2008**, *14*, 4810-4815.

(24) Novakova, V.; Reimerova, P.; Svec, J.; Suchan, D.; Miletin, M.; Rhoda, H. M.; Nemykin, V. N.; Zimcik, P. Systematic investigation of phthalocyanines, naphthalocyanines, and their aza-analogues. Effect of the isosteric aza-replacement in the core. *Dalton Trans.* **2015**, *44*, 13220-13233.

(25) Makhseed, S.; Tuhl, A.; Samuel, J.; Zimcik, P.; Al-Awadi, N.; Novakova, V. New highly soluble phenoxy-substituted phthalocyanine and azaphthalocyanine derivatives: Synthesis, photochemical and photophysical studies and atypical aggregation behavior. *Dyes Pigm.* **2012**, *95*, 351-357.

(26) Stuzhin, P. A.; Malyasova, A. S.; Sheinin, V. B.; Kokareva, E.; Tarakanov, P. A.; Koifman, O. I. Acid-base properties of tetrapyrazinoporphyrazines. 1. Deprotonation of octaethyltetrapyrazinoporphyrazine in CH_2Cl_2, THF, DMSO and pyridine. The crucial role of water. *Dyes Pigm.* **2017**, *139*, 509-516.

(27) Petrik, P.; Zimcik, P.; Kopecky, K.; Musil, Z.; Miletin, M.; Loukotova, V. Protonation and deprotonation of nitrogens in tetrapyrazinoporphyrazine macrocycles. *J. Porphyrins Phthalocyanines* **2007**, *11*, 487-495.

(28) Michelsen, U.; Kliesch, H.; Schnurpfeil, G.; Sobbi, A. K.; Wöhrle, D. Unsymmetrically substituted benzonaphthoporphyrazines: A new class of cationic photosensitizers for the photodynamic therapy of cancer. *Photochem. Photobiol.* **1996**, *64*, 694-701.

(29) Tuhl, A.; Makhseed, S.; Zimcik, P.; Al-Awadi, N.; Novakova, V.; Samuel, J. Heavy metal effects on physicochemical properties of non-aggregated azaphthalocyanine derivatives. *J. Porphyrins Phthalocyanines* **2012**, *16*, 817-825.

(30) Novakova, V.; Laskova, M.; Vavrickova, H.; Zimcik, P. Phenol-substituted tetrapyrazinoporphyrazines: pH-dependent fluorescence in basic media. *Chem.-Eur. J.* **2015**, *21*, 14382-14392.

(31) Cruess, A. F.; Zlateva, G.; Pleil, A. M.; Wirostko, B. Photodynamic therapy with verteporfin in age-related macular degeneration: a systematic review of efficacy, safety, treatment modifications and pharmacoeconomic properties. *Acta Ophthalmol.* **2009**, *87*, 118-132.

(32) Senge, M. O.; Brandt, J. C. Temoporfin (Foscan®, 5,10,15,20-tetra(*m*-hydroxyphenyl)chlorin)—A second-generation photosensitizer. *Photochem. Photobiol.* **2011**, *87*, 1240-1296.

(33) Kennedy, J. C.; Pottier, R. H. Endogenous protoporphyrin IX, a clinically useful photosensitizer for photodynamic therapy. *J. Photochem. Photobiol., B* **1992**, *14*, 275-292.

(34) Machacek, M.; Kollar, J.; Miletin, M.; Kucera, R.; Kubat, P.; Simunek, T.; Novakova, V.; Zimcik, P. Anionic hexadeca-carboxylate tetrapyrazinoporphyrazine: synthesis and in vitro photodynamic studies of a water-soluble, non-aggregating photosensitizer. *RSC Adv.* **2016**, *6*, 10064-10077.

(35) Saftig, P.; Klumperman, J. Lysosome biogenesis and lysosomal membrane proteins: trafficking meets function. *Nat. Rev. Mol. Cell Biol.* **2009**, *10*, 623-635.

(36) Vanlandingham, P. A.; Ceresa, B. P. Rab7 regulates late endocytic trafficking downstream of multivesicular body biogenesis and cargo sequestration. *J. Biol. Chem.* **2009**, *284*, 12110-12124.

(37) Rottger, S.; White, J.; Wandall, H. H.; Olivo, J. C.; Stark, A.; Bennett, E. P.; Whitehouse, C.; Berger, E. G.; Clausen, H.; Nilsson, T. Localization of three human polypeptide GalNAc-transferases in HeLa cells suggests initiation of O-linked glycosylation throughout the Golgi apparatus. *J. Cell Sci.* **1998**, *111 (Pt 1)*, 45-60.

(38) Huang, J.-D.; Lo, P.-C.; Chen, Y.-M.; Lai, J. C.; Fong, W.-P.; Ng, D. K. P. Preparation and in vitro photodynamic activity of novel silicon(IV) phthalocyanines conjugated to serum albumins. *J. Inorg. Biochem.* **2006**, *100*, 946-951.

(39) Sharman, W. M.; van Lier, J. E.; Allen, C. M. Targeted photodynamic therapy via receptor mediated delivery systems. *Adv. Drug Delivery Rev.* **2004**, *56*, 53-76.

(40) Perrin, D. D.; Armarego, W. L. F. *Purification of Laboratory Chemicals*; 4th ed.; Butterworth Heinemann: Oxford, Boston, 1997.

(41) Novakova, V.; Miletin, M.; Filandrová, T.; Lenčo, J.; Růžička, A.; Zimcik, P. Role of steric hindrance in the Newman-Kwart rearrangement and in the synthesis and

photophysical properties of arylsulfanyl tetrapyrazinoporphyrazines. *J. Org. Chem.* **2014**, *79*, 2082-2093.

TABLE OF CONTENT GRAPHIC

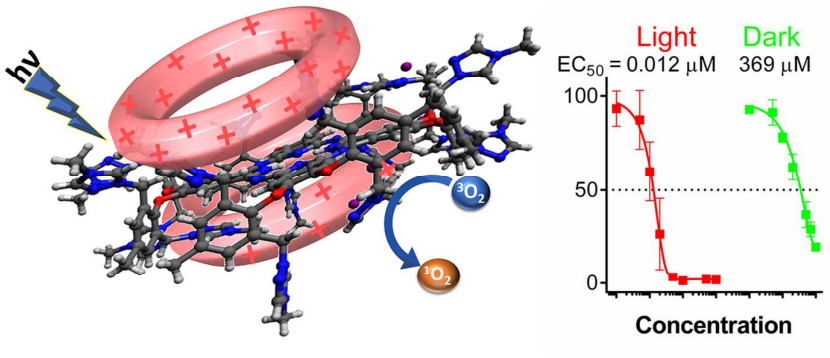

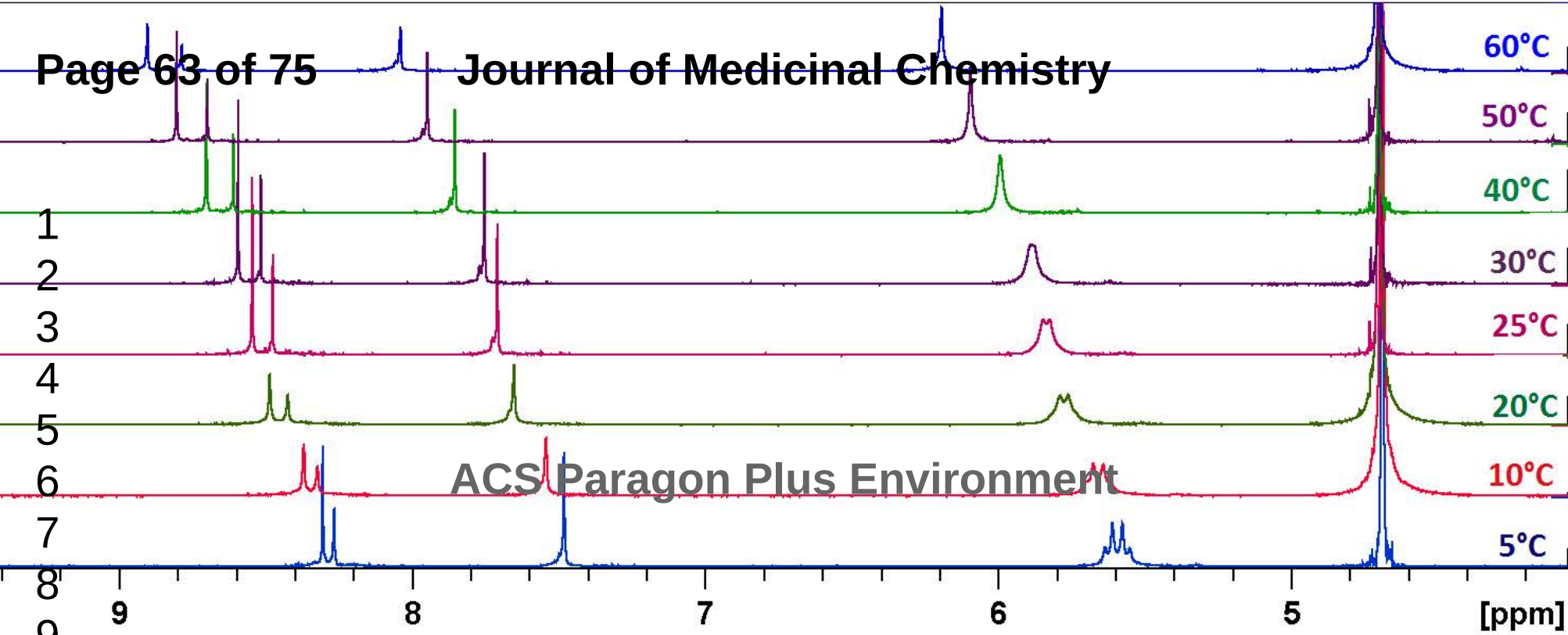

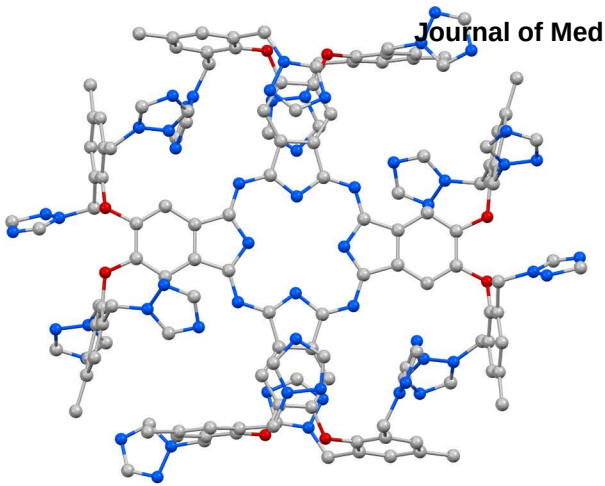

7A

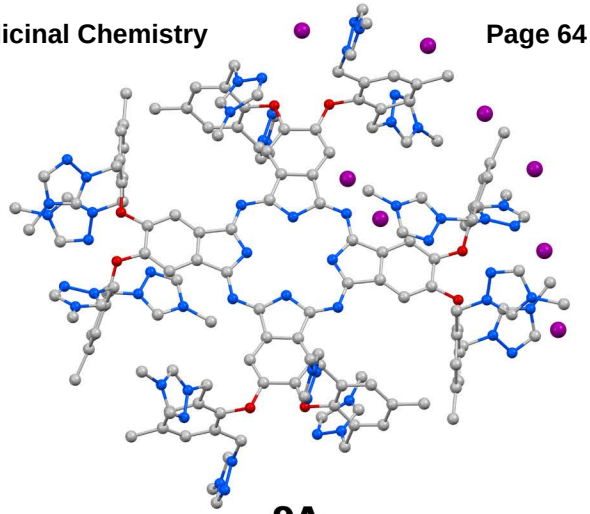

9A

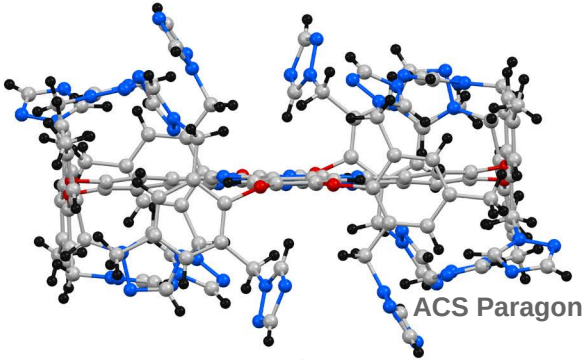

7B

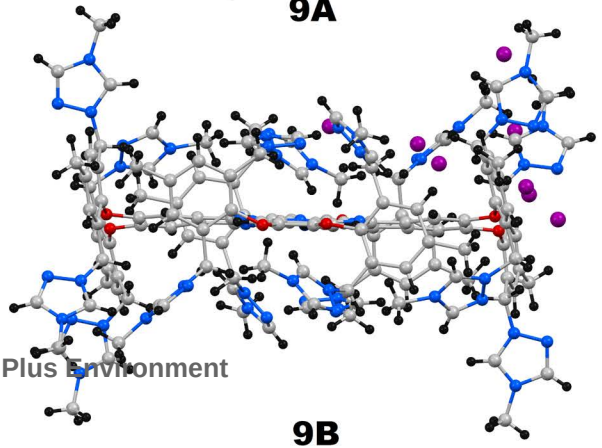

9B

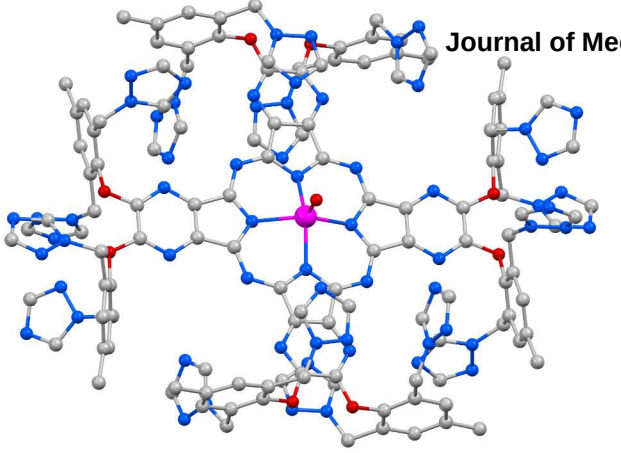

11A

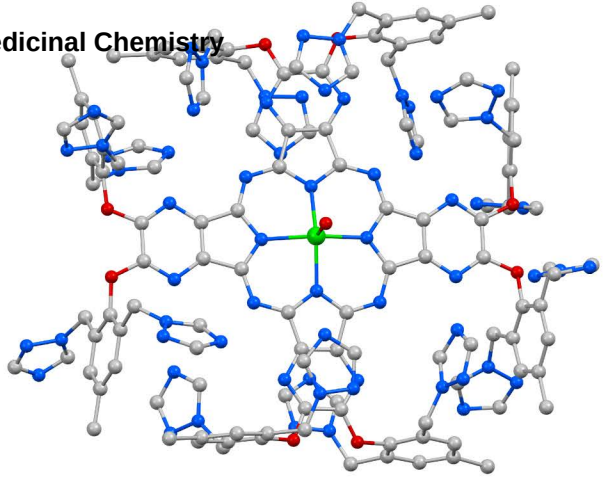

13A

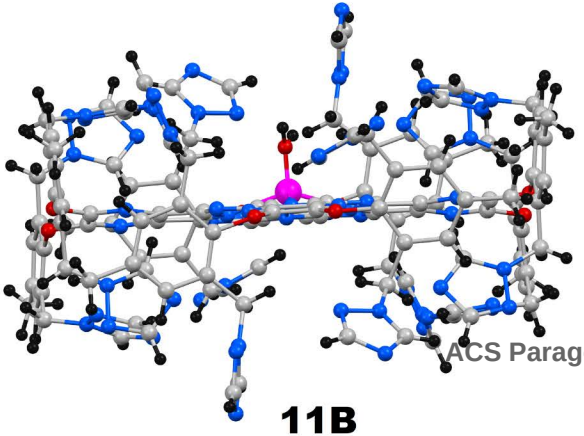

11B

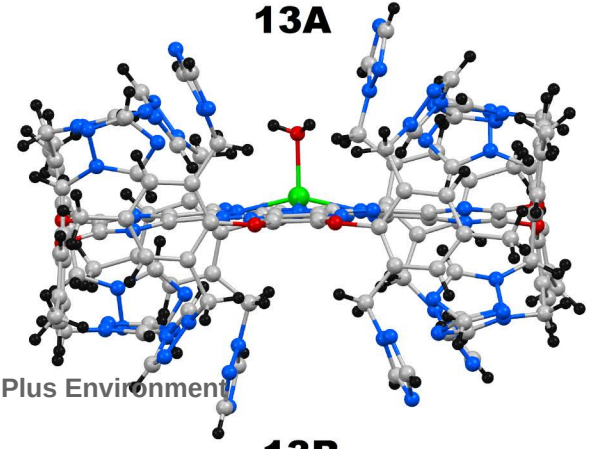

13B

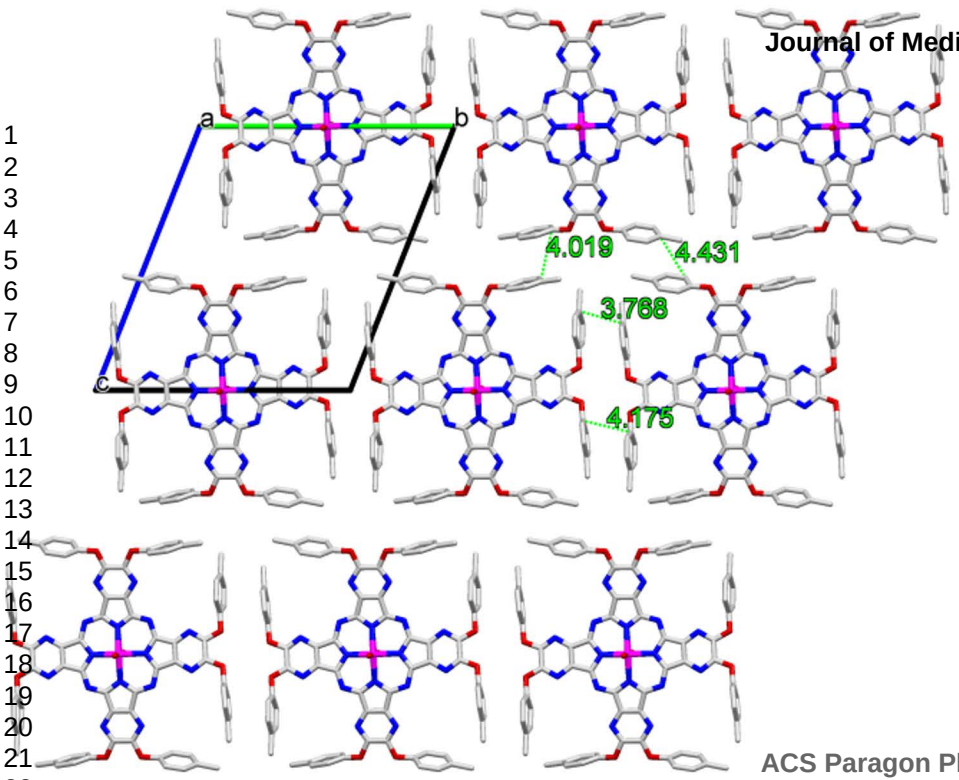
a
b
c
4.019
4.431
3.768
4.175

A

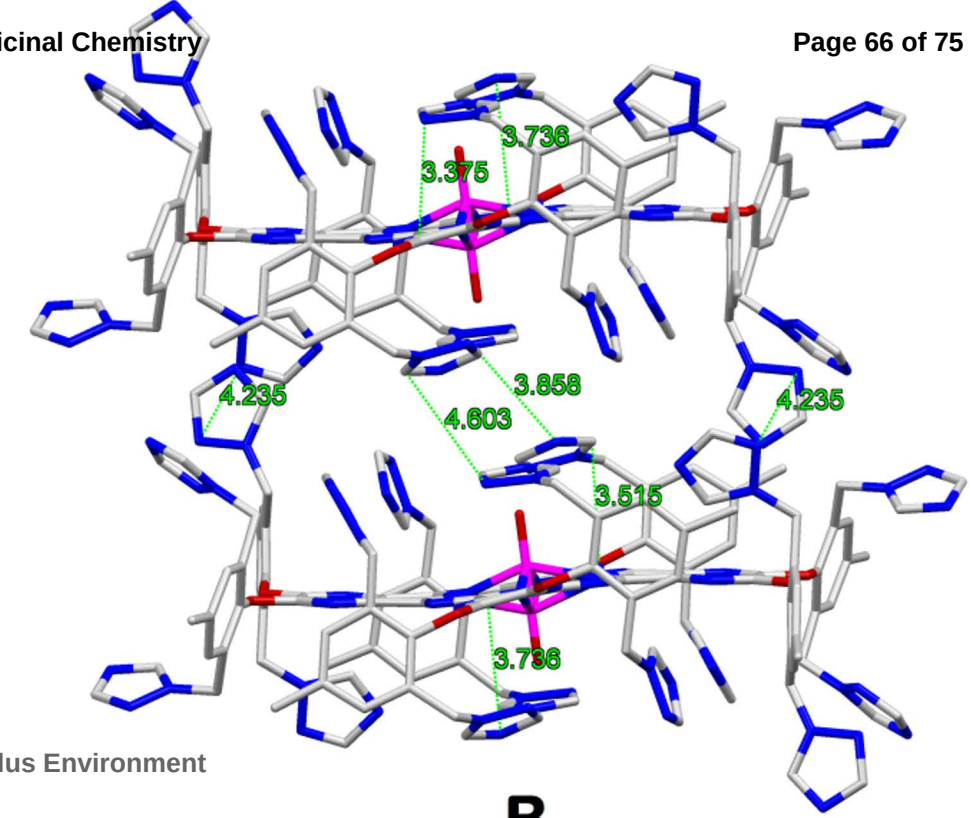
3.736
3.375
4.235
3.858
4.603
4.235
3.515
3.736

B

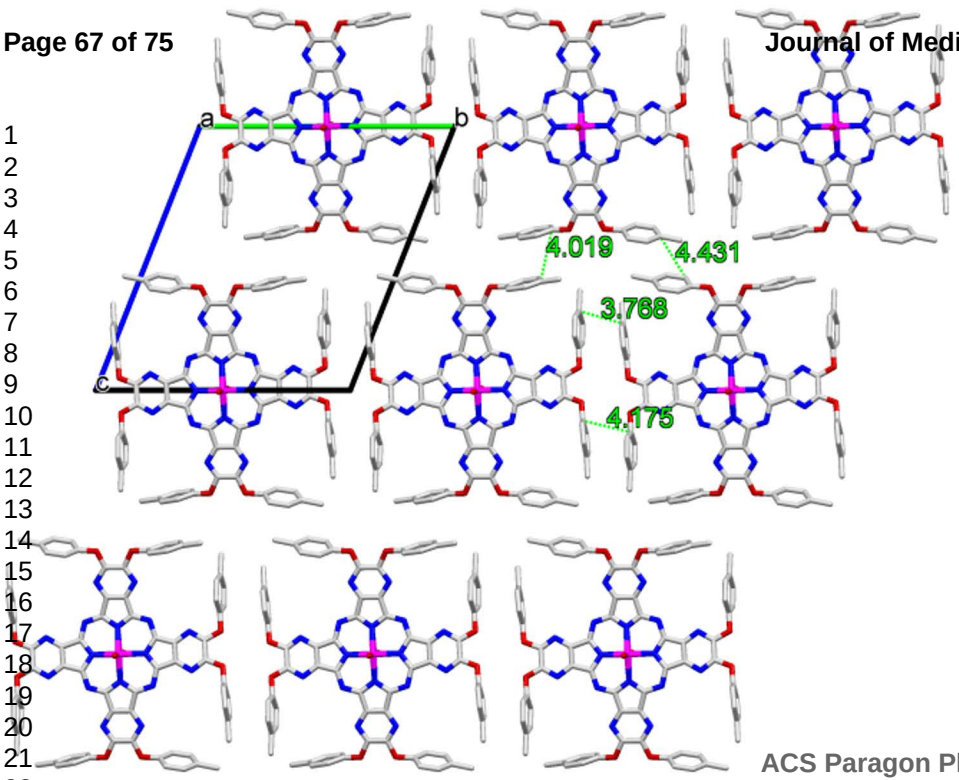

A

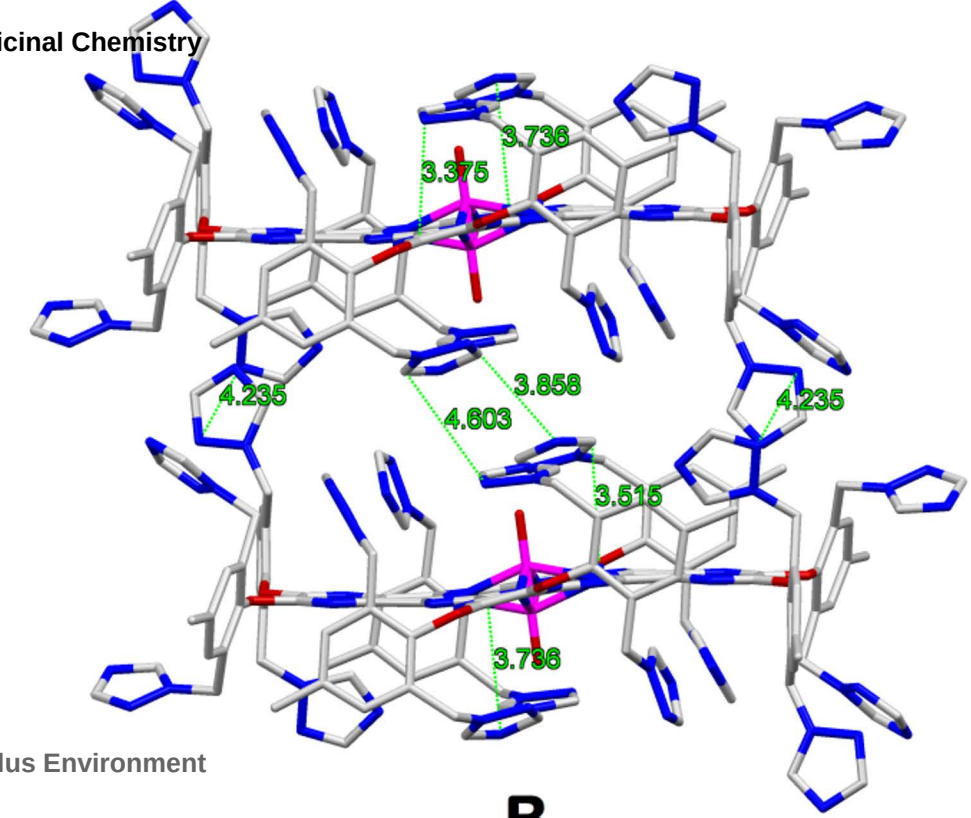

B

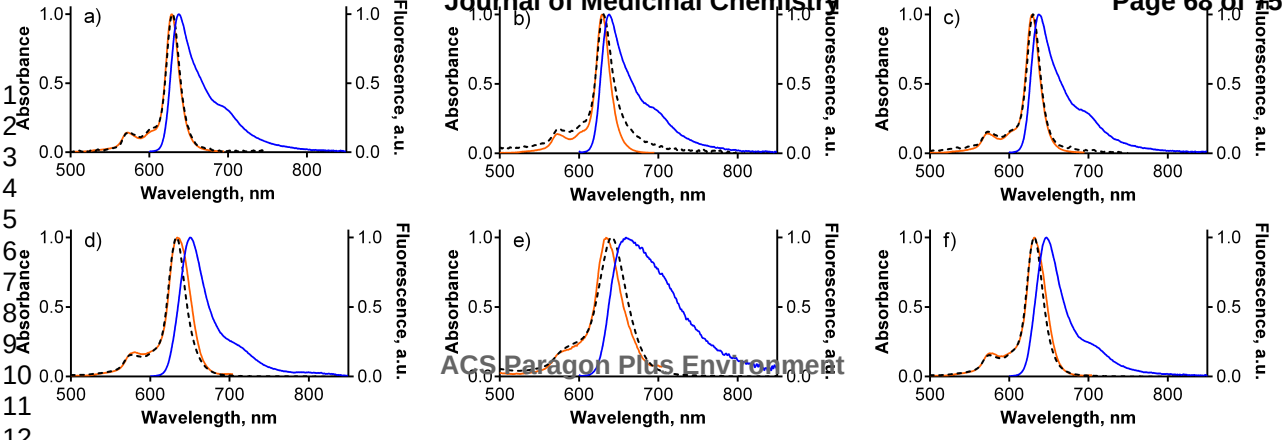

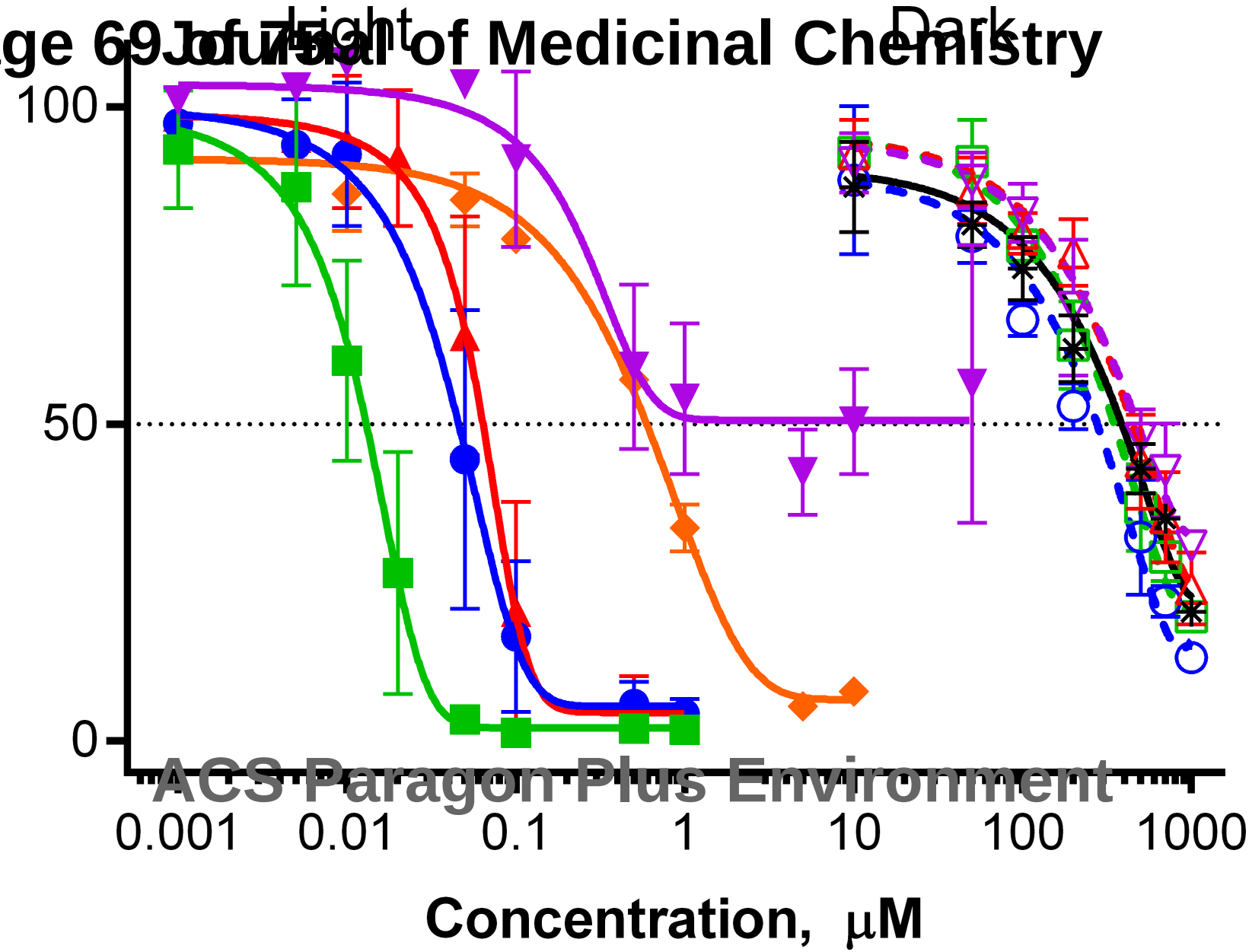
Light
Dark
100
50
0
Viability, % of control
0.001
0.01
0.1
1
10
100
1000
Concentration, μM
ACS Paragon Plus Environment